Multiscale Modeling Unravels the Influence of Biomembranes on the Photochemical Properties of Embedded Anti-Oxidative Polyphenolic and Phenanthroline Chelating Dyes

Benetis, Nikolas P.; Paloncyova, Marketa & KNIPPENBERG, Stefan (2022) Multiscale Modeling Unravels the Influence of Biomembranes on the Photochemical Properties of Embedded Anti-Oxidative Polyphenolic and Phenanthroline Chelating Dyes. In: JOURNAL OF PHYSICAL CHEMISTRY B, 127 (1) , p. 212 -227.

DOI: 10.1021/acs.jpcb.2c07072
Handle: http://hdl.handle.net/1942/39352

Multiscale Modeling Unravels the Influence of Biomembranes on the Photochemical Properties of Embedded Anti-oxidative Polyphenolic and Phenanthroline Chelating Dyes

Nikolas P. Benetis,[1,*] Markéta Paloncýová,[2] Stefan Knippenberg,[3,4]

[1] University of Western Macedonia, kila Kozani, 501 00, Greece

[2] Regional Centre of Advanced Technologies and Materials, Czech Advanced Technologies and Research Institute, Palacký University Olomouc, Křížkovského 8, Olomouc 779 00, Czech Republic;

[3] Hasselt University, Theory Lab, Agoralaan Building D, 3590 Diepenbeek, Belgium

[4] Université Libre de Bruxelles, Spectroscopy, Quantum Chemistry and Atmospheric Remote Sensing (SQUARES), 50 Avenue F. Roosevelt, C.P. 160/09, B-1050 Brussels, Belgium

* Author to whom correspondence should be sent: Nikolas P. Benetis, n.mpenetis@uowm.gr

Abstract

The embedding of caffeate methyl ester, the flavonoids luteolin and quercetin, as well as the o-phenanthroline and neocuproine in a liquid disordered lipid bilayer has been studied through extensive atomistic calculations. The location and the orientation of these bio-active antioxidants are explained and analyzed. While the two phenanthrolines strongly associate with the lipid tail region, the other three compounds are rather found among the head groups. The simulations showcase conformational changes of the flavonoids. Through the use of a hybrid Quantum Mechanics – Molecular Mechanics scheme and supported by a profound benchmarking of the electronic excited state method for these compounds, the influence of the anisotropic environment on the compounds' optical properties is analyzed. Influences of surrounding water molecules and of the polar parts of the lipids on the transition dipole moments and excited state dipole moments are weighted

with respect to a change in conformation. The current study highlights the importance of the mapping of molecular interactions in model membranes and pinpoints properties which can be biomedically used to discriminate and detect different lipid environments.

Introduction

Plant- origin foods like fruit, vegetables and beverages like tea, as well as red wine contain polyphenolic compounds like flavonoids that are associated with health maintenance and the prevention of chronic and degenerative diseases[1,2,3].The Mediterranean diet is based in olive oil, a source of fatty acids, and in addition rich in fruits and vegetables. Olive oil contains a number of phenolic compounds which are responsible for its stability to oxidative rancidity. Many of these components such as e.g. tyrosol, hydroxytyrosol, oleuropein, caffeic acid, flavonoids are regarded as strong antioxidants and radical scavengers[1,4,5,6].

Flavonoids form a large group of more than 6000 phenolic compounds differing in the number of hydroxyl groups attached to their benzo-γ-pyrone ring complex. They are found in several species of the plant kingdom, and are known to possess strong antioxidant activity[1,7,8,9]. A number of flavonoids belonging to the flavone, flavonol, flavanone, and flavan-3-ol subclasses protect cellular DNA from H_2O_2-induced single-strand breaks[10,11,12]. In addition, the use of flavonoids as natural metal chelators should be favored as pharmaceutical cytoprotectives against other synthetic metal-ion chelators which may present some problems of toxicity.

The five molecules to be studied here and a series of similar substances belonging to the above categories are known to protect the cell from the detrimental oxidation effect of free iron ions by impeding the Fenton reaction[1,4]. Aspects of underlying protection mechanism have been investigated by biochemistry methods developed by several groups, see[13,14,15,16] and references there. Experimental biochemistry studies demonstrated that cytoprotection against H_2O_2-induced cellular DNA damage was achieved after pre-incubation of the cells with specific Fe- or Cu- ion chelators able to penetrate in the cell membrane[1,17,18]. The five antioxidant dyes that were chosen in this work were under incubation with cell cultures hindering single strand DNA breakage from hydrogen peroxide in presence of iron and/or copper ions[13]. They are

all small planar amphiphilic bidental metal –ion chelators displaying an extensive conjugated double bond system amenable to theoretical and experimental spectroscopic studies and detection. The above common features, as well as their cell membrane affinity, are all found to be related to the mechanism of the above of the cell DNA protection.

It was further observed that effective protection was based on the ability of the compound to (i) reach the intracellular space and, (ii) chelate intracellular "labile" iron. However, the molecular mechanism underlying the health keeping effects of the cell still remains unknown. The membrane interaction of the chelating sites of small dyes as a link to their known experimental antioxidant activity will be studied in this work.

The chelating ability of the antioxidants of the present work was verified previously for different systems[19,20,21]. Characteristic is the protective ability from DNA damage of the 1,10-phenanthroline (oPhen) chelator against its non-chelating isomer 1,7-phenanthroline that provided no protection[22,13]. A totally different system, hydroxy tyrosol (3,4-dihydroxyphenylethanol) with two adjacent chelating phenolic hydroxyls, but not Tyrosol, was able to protect cells in culture from H_2O_2-induced of single strand breaks formation in nuclear DNA as was shown in[1, 23, 24] and references there.

The flavonoids Luteolin (Luteo) and Quercetin (Querc) possess a couple of possible bidental chelating sites consisting of adjacent phenolic or mixed phenolic-ketonic pairs of oxygen atoms easily discerned in Figure 1. One phenolic chelating site and molecular flexibility similar to flavonoids is shared by the smaller molecule of the methyl caffeate ester (Caffest). The molecules of o-Phenanthroline (oPhen) and the Neocuproine (Neocu) possess also bidental chelating sites based instead on two adjacent nitrogen atoms, Figure 1. The active electron pairs of the chelating oxygen or nitrogen extremities of the above species are important as they can act as polar extensions attracted by the membrane zwitterionic headgroup and/ or the water molecules associated to it.

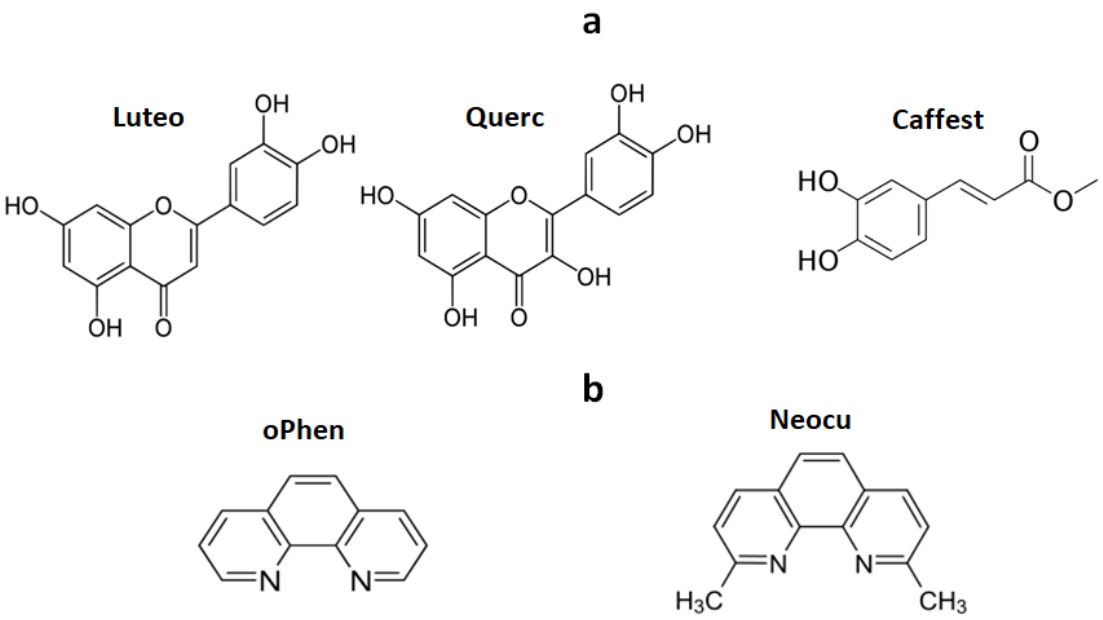

Figure 1. a*:* The flavonoids luteolin (Luteo) to the left and quercetin (Querc) in the middle are depicted in this figure with the smaller molecule of caffeate methyl ester (Caffest) seen to the right. The phenolic-aromatic A- and catechol B- outer rings of the two flavonoid molecules are separated from the middle pyrone C- ring. The planar surface formed by the combination of the A-and the pyrone C- rings will be referred further as pyrone complex. **b***:* The two phenanthrolines, o-phenanthroline (oPhen) in the left and neocuproine (Neocu) to the right.

Relevant studies of similar antioxidants show that the prominent properties in common of the above mentioned groups of substances is their membrane affinity, the chelating ability as well as the planarity due to an extensive conjugated double bond system.

The bidental chelator caffeic acid derivatives are particularly active as cytoprotectives due to their small size and the affinity to the cell membrane. However, the caffeic acid itself, which is negatively charged at neutral pH, was largely ineffective, even at relatively high concentrations, although able to chelate iron[25,26]. Caffeate methyl ester (Caffest) on the other hand, that is one of the targets of the present work, displayed increased protective ability with the carboxyl group neutralized by esterification, thus easier penetrating plasma membrane.

A systematic presentation of the energies and the structural parameters for different iron- complexes of several flavonoids can be found in[27]. In particular the optical properties of free quercetin and its iron adducts were computed using Density

Functional Theory (DFT) methods. The changes of optical absorption of the quercetin molecule by the metal-ion complexation were also identified, explained and compared with experimental data[27].

Lipid membranes are fundamental components of life as they conditionally separate and/or bring in contact the cell to the immediate environment allowing only specific functions of life to occur related chiefly with the exchange of matter and energy. Their functionality is regulated by their phase, either solid (S_o), liquid ordered (L_o) or liquid disordered (L_d). Most of the parameters determining the phase of the model membranes such the lateral diffusion coefficient D_L and the order parameter of the alkyl chains $<Y_{20}(\theta)>$ can be derived using Molecular Dynamics (MD) simulations (Table S1). Standard thickness and the area per lipids literature data[28] can also be used to assess the phase of model membranes MD computation results.

The phase of the model membranes depends on the composition, either only a single lipid or a lipid in mixture usually with cholesterol facilitating the formation of the L_o phase, and the temperature. In particular, Ploeg and Berendsen[29] have early correlated the dynamics of increased bilayer order to the collective tilt of the acyl chains as the model membrane comes in to the gel S_o phase.

High resolution Magic Angle Spinning Nuclear Magnetic Resonance (MAS NMR) methods and two-dimensional polarization-enhancement methods improving over the years have been used for studying flavonoid-model membranes interaction (See[30] and references therein). For example ^{1}H NMR techniques and pulsed field-gradient NMR measurements were used[8] to investigate the properties of four flavonoids with different number of phenolic hydroxyls per molecule in 1-Palmitoyl-2-oleoylphosphatidylcholine (POPC) model membrane. The relation between hydrophobicity and membrane localization/orientation, as well as measurements of the lateral diffusion coefficients of the membrane lipids were obtained in that work. The four flavonoids were shown to be distributed differently inside the lipid core along the membrane normal depending on the number of hydroxyl groups with a maximum probability at the lipid/water interface for those with most hydroxyls.

There is still a question where certain flavonoids are located in a membrane[31]. In that study the effects of flavonoids, isoflavonoids, and their metabolites on membrane fluidity is investigated using large unilamellar vesicles (LUVs) as the membrane model. It was further postulated that the studied flavonoid species were preferentially confined in the hydrophobic core where they increase the fluidity in the membranes.

In the present work it is on the contrary certified that the flavonoids Luteo and Querc not only avoid the hydrophobic core but they are instead firmly in contact with the hydrophobic edge of the headgroup interacting with the water content of the hydrophilic 1,2-dipalmitoyl-sn-glycero-3-phosphocholine (DPPC) model membrane zone. In the current paper, it is not our aim to evaluate the flavonoid load on the membrane fluididity. Instead, the influence of the membrane environment on the behavior and the properties of a single flavonoid molecule is investigated.

The optical properties of the five probes embedded in L_d model membranes are studied in this report. MD simulations and hybrid Quantum and Molecular Mechanics (QM/MM) calculations of the molecules in the lipid bilayer consisting of DPPC/water are evaluated and tested.

The choice of DPPC as a model membrane at 323K (50 ^oC) was made to enable a calculation in L_d phase while maintaining the saturated tails of phosphatidylcholine (PC) lipid. PC lipids are the most abundant lipids in mammalian cell membranes[32] and are known as the simplest cell membrane models. We used saturated lipids for simplicity, in order to focus on lipid type defined by lipid head group and avoid a discussion on the spurious influence of unsaturated parts eventually present in the tails. The results in the current work can furtheron be compared to other studies which have been performed in similar conditions and which focus on the influence of the membrane on the probe's conformation, position and orientation[33,34].

The overall planarity conditions of the more flexible Caffest and the flavonoids are estimated against the potential they are sensing in the environment, isotropic (gas phase) or membrane embedding. Hybrid QM/MM calculations are employed to understand how they perform with respect to two different optical spectroscopies, one- and two-photon absorption, OPA and TPA, respectively. The OPA spectra are based on linear response calculations, while the non-linear TPA spectra relate to the first residue of the quadratic response function. This methodology of the optical properties has been validated for several dyes embedded in both solid phase DPPC and liquid crystalline 1,2-dioleoyl-sn-glycero-3-phosphocholine (DOPC) model membranes[35,36,37,38].

A promising start for a theoretical investigation disentangling the above kind of cell protection mechanism from H_2O_2-induced single-strand DNA damage would be to study first the chelating dyes in membrane environment. These active chromophores can be used as non-invasive probes revealing information about the environment: due

to their specific locations and orientations in the membrane, the interaction of the surrounding biological material changes and influences the (non-) linear absorption spectra.

The current manuscript is constructed as follows. After an overview of the computational details of the current study, the results are given. The position and orientation of the probes in the membrane is investigated by means of MD calculations. Special attention is paid to the transition dipole moments in these compounds, which are responsible for their optical response in a supported lipid bilayer membrane. Hybrid QM/MM calculations are performed and provide the opportunity to discuss the use of these molecules in optical experiments. The influence of the molecular conformation on the spectra and of the environment on the linear and non-linear optical properties of the molecules is investigated. Finally, the conclusions of this work are concisely given.

Computation Details

All the MD calculations have been performed with the GROMACS simulation package[39]. The parameters describing the simulation conditions and the energy minimization are shown in the files md.mdp and em.mdp, respectively, in the SI. A pre-equilibrated lipid bilayer has been considered as a model membrane, made of 50 DPPC molecules per layer, solvated in 3205 water molecules and neutralized with a physiological concentration of counter ions. One probe molecule per simulation was added initially to solvent layer (water) on the top of the simulation box, not interacting with the membrane, parallel to the membrane/ water interface.

For all five probe molecules studied here, the partial charges in vacuum were obtained with the Electrostatic Potential (ESP) scheme implemented in the Gaussian09 program along with the B3LYP functional and cc-pVDZ basis set[40,41,42,43]. This charge description has been chosen since it provides an accurate model for the simulation of lipid bilayer systems. Both the lipids and the probe molecules were modeled by a GROMOS 43a1-s3 force field[44], while water was taken into consideration via the SPC/E model. The time step for the integration of the equation of motion was 2 fs, all-bonds constraints were kept with the LINCS algorithm[45]. Coulombic and van der Waals interactions were treated explicitly to 1.4 nm, further, the Particle Mesh Ewald (PME) method was applied for electrostatic interactions[46].

An orthorhombic box of 56.859 × 56.068 × 68.574 Å^3 has been considered for the probes in the DPPC–water bilayer. To maintain the L_d phase, the simulations have been performed in the canonical NPT ensemble at 323 K using the Parrinello−Rahman barostat (semi-isotropic, 1 bar, with a time constant of 5 ps and compressibility 4.5 × 10^{-5} bar^{-1}) and Nosé-Hoover thermostat[47, 48]. We performed the simulations for ~240 and ~370 ns, enough for the probes to enter the membrane aliphatic zone and obtain a reasonable equilibrium period used in the properties' computations.

In the next step, the MD simulations were further used to obtain the OPA and the TPA spectra both in vacuum and embedded in the DPPC model membrane. For each of the five probes, 40 uncorrelated, evenly distributed snapshots were extracted from the equilibrated MD simulations to obtain the input for the QM/MM calculations within the electrostatic embedding method implemented in the Dalton2016 package of programs[49]. In this scheme, the system is divided into two parts, in which the probe is described at the Time-Dependent Density Functional Theory (TDDFT) level of theory. We extracted by a cylindrical cutoff of 1.2 nm the lipids around the probes and used a corresponding semispherical cutoff for the solvent. The same QM part of the computation was repeated for vacuum conditions by disregarding the electrostatic MM potential. The optical properties of the four lowest excited states of the dyes have been considered for the OPA and the–TPA spectra computations using the CAM-B3LYP functional and Dunning's cc-pVDZ basis set[50].

The two-photon transition amplitudes can be identified with the residues of a quadratic response function. The two-photon transition matrix elements along with the two-photon transition probability are in principle connected with the imaginary part of the second hyper-polarizability[51,35].

A useful property for fluorescent microscopy is the cross section sigma of the two-photon TPA absorption, σ_{TPA}, measured in Goeppert-Mayer units (1 GM = 10^{-50} cm^4 /photon), and computed as[35],

$$\sigma_{TPA} = \frac{8\pi^3 \alpha^2 h/2\pi}{e^4} \omega^2 \delta_{TPA}^f \qquad (1)$$

where α is the fine constant, $h/2\pi$ is the reduced Planck constant h-bar, e the elementary charge and ω is the OPA excitation energy. The TPA transfer probability δ_{TPA}^f is computed as[52, 53]:

$$\delta_{TPA}^{f} = \sum_{\alpha\beta}\left[\frac{1}{15} S_{\alpha\alpha}^{f} S_{\beta\beta}^{f\,*} + \frac{2}{15} S_{\alpha\beta}^{f} S_{\beta\alpha}^{f\,*}\right] \quad (2)$$

The intermediate energies (ω_i) of the intermediate states (i) for the transitions from the ground (0) to the excited (f) state must be considered in the two photon matrices $S_{\mu\nu}^{f}\, S_{\alpha\beta}^{f}$ which are given as:

$$S_{\alpha\beta}^{f} = \sum_{i}\left[\frac{\langle 0|\mu_\alpha|i\rangle\langle i|\mu_\beta|f\rangle}{\omega_i - \omega_f/2} + \frac{\langle 0|\mu_\beta|i\rangle\langle i|\mu_\alpha|f\rangle}{\omega_i - \omega_f/2}\right] \quad (3)$$

The absorption cross sections are evaluated assuming a monochromatic light source that is either linearly or circularly polarized.

Results

The MD simulations start with one probe molecule solvated in the water zone ca 4 nm from the middle of the membrane. During the simulation process the distance of the drug molecule from the middle of the membrane is monitored. Although all five simulations started from the same position of the same leaflet the traces of Caffest and Querc were separated in Figure 2 and Figure S1 avoiding curve crowding in the same plot. All five drugs entered the membrane within the first 70-100 ns, passing quickly through the headgroup and stayed predominantly in at the vicinity of the lipid-core/headgroup interface. It was found that after certain simulation time shown in Table S2, the probes were able to reach equilibrium in the studied DPPC/water/drug environment. Equilibration in the present context means that the probes stay in average at the same location of the membrane for the rest of the simulation, incorporated in the aliphatic zone of the membrane. During the equilibrium stage the orientation of the small probes was reasonably fluctuating allowing their orientation average computation. Figure S2 shows the fluctuation of the Caffest during the MD simulations representing the behavior of the five studied dyes, assessing the beneficial time window out of the total MD simulation period shown in Table S2. In a time window beyond 300 ns, it can be seen that Neocu permeates to the other membrane leaflet. When the time window would be extended, it is logical to obtain two symmetrical densities for this molecule in both symmetrical leaflets. As the oPhen probe is smaller than Neocu and with respect to the identical lipophilic body, it is tempting to say that for oPhen a leaflet flip is also expected when the MD run is extended. However, in Neocu the polar nitrogen tips are shielded by the lipophilic

methyl groups, which is not true for oPhen. Also, as we proved in previous works on azobenzene and cyanine derivatives, the tails of the inserted probes have a profound influence on the position and orientation: it was found that they can have a pulling as well as pushing effect[33,34]. Within the limits of the here reported calculations and the used time windows, the difference between the two probes might thus be attributed to the extra methyl groups present which pull dynamically the Neocu towards the middle of the membrane.

MD Simulations of Antioxidants in DPPC Membrane

All five antioxidant probes entered the membrane within the first 100 ns of ca. 340 ns MD simulations and remained close to the lipid core/headgroup interface (Figure 2 and S2). Luteo and Caffest were found outermost in the membrane, with their center of masses at ca. 1.2 nm away from the membrane center. We remark that these results are obtained by dynamical computations and are not the result of Gibbs free energy calculations, which can for instance be obtained by the z-constraint method[54, 55], which has been used in the past to shed light upon the affinity of probes for different membranes[56]. The oPhen chelator can be found innermost of all the concerned probes (0.7 nm). The values of the structural and dynamics parameters, the average thickness, the area per lipid, the lateral diffusion constant and the order parameter shown in the supporting information (Figure S3 and S4) are representative for the L_d phase of DPPC membrane. Therefore it is most easily permeable for drugs and indeed, we observed that Neocu due to the extra lipophilicity of the two methyl-group substituents (but not the somewhat smaller oPhen) freely permeated to the opposite leaflet (Figure S1). There it equilibrated again under the headgroup region, symmetrically at the same position as in the original leaflet.

The preferential interaction with the lipid membrane supports the possibility of antioxidant membrane penetration, which is necessary for its antioxidant effect[17], though we did not observe any reemerging of a probe back into water region (Figure S1). The penetration can be achieved either passively or with an active penetration mechanism. In case of e.g. Caffeic acid and its esters, it could be hindered by their hydrophilic character[57]. But for hydrophobic molecules, the permeation can happen via accumulation of these molecules in the membrane and changing the membrane properties, e.g. lower the phase transition temperature as observed with Querc[1], or

directly increase membrane fluidity[31]. In conclusion, all studied probes stayed in the lipid membrane for the whole simulation time and we can further describe the lipid effect on their behavior.

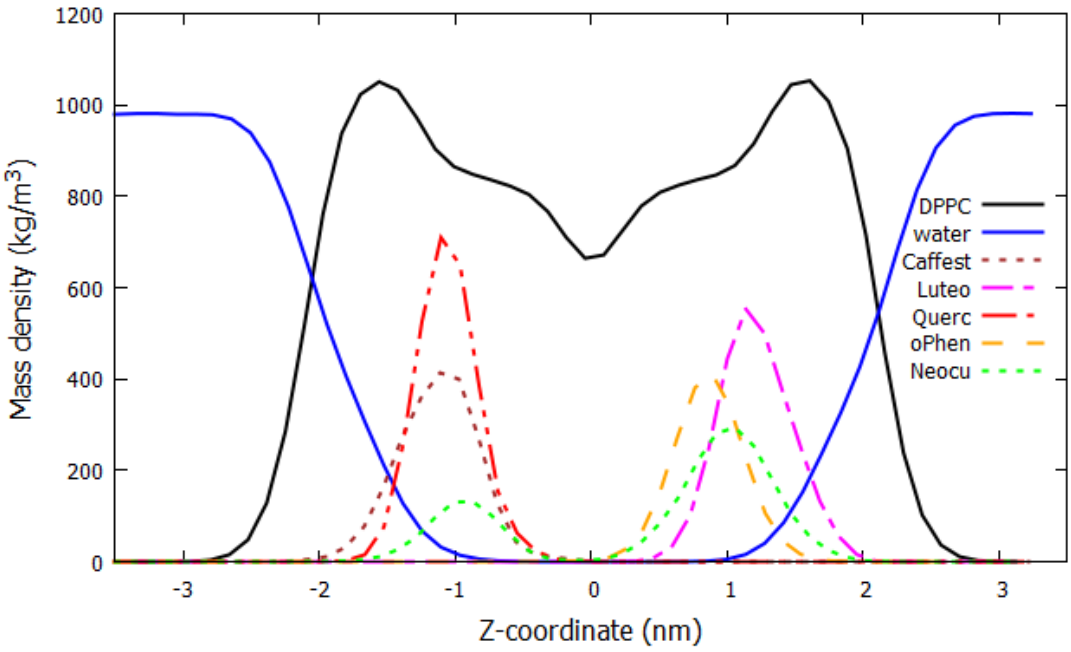

Figure 2. All drug densities' histogram in the DPPC membrane framework. The density profiles of all the main parts of the bilayer/ water/ drug system are shown along the Z-axis perpendicular to membrane surface. Avoiding curve crowding in the figure the MD simulation of Caffest and Querc simulations started from the opposite edge of the symmetrical membrane.

Structure vs. Membrane/ Probe Interaction

While phenanthrolines are fully rigid molecules, flavonoids consist of two planar aromatic- ring units connected with a hybrid single/double bond. The assignment of force field parameters made this bond rotatable (Figure 3), as was observed for Luteo, while Querc rotation was hindered by a phenolic hydroxyl group.

In Figure 3 is shown the distribution of the intramolecular pyrone/ catechol dihedral angle of Querc. It does not change sign throughout the entire MD simulation, while the dihedral angle for Luteo oscillates about zero degrees. The dihedral angle of Querc spans over all conformations in the 0 to 180 degrees range, with a maximum at 78 degrees, indicating a dominating non-planar conformation with the two aromatic rings of the molecule nearly perpendicular. On the contrary, Luteo conformation

alternate between dihedral angles +/-54 and +/-67 degrees, allowing statistically the planar conformation. Assuming standard normal distribution, eq. (S3), the dihedral angle plot in Figure 3 can be interpreted as following: the probability for Querc to obtain 90 degrees in the interval 0 to 180 degrees is 0.804 or about 80% while the probability of Luteo to obtain an angle of +/- 60 degrees in the interval -180 to 180 is 0.587 or ca 59 %.

The distorted conformation of the two flavonoids is also obvious in the DPPC model membrane framework depicted in the snapshots of Figure S5. We are aware, that later QM calculations showed the preference to planar conformation with ca 6.2 kcal/mol barrier (Figure S6A) and the calculated optical properties could be affected, but we believe that the nature of antioxidant-membrane interactions remained intact. Furthermore the greater rotation barrier by ca 2.1 kcal/mol for Querc vs. Luteo about the 90 degrees dihedral angle is in agreement with the easier passage of Luteo about the planar configuration compared to Querc shown in Figure 3.

One should distinguish the physical meaning of the QM barrier computation of Figure S6A from the MD computation in Figure 3. The first describes the energy that the static molecule would acquire for the chosen input angles. On the contrary, Figure 3 simulates the dynamics occurring for a system in “real” conditions under the influence of thermal motion and in connection to the interaction of the molecule with the membrane environment.

We computed the OPA transitions of Querc and Luteo for the 0 and 90 degrees conformers. As can be seen in Table S7 the S1 and S2 excitations of Luteo are degenerated for 0°, while they are rather clearly separated for 90°. Notice that the strongly allowed S1 peak for Querc blue shifts with more than 25 nm when the angle is changed from 0 to 90°. These data give also another proof of our statement: the longer the conjugated double bond system the smaller the transition frequency. It is indeed seen that all the 0 degrees (planar conformation) transitions are smaller in frequency.

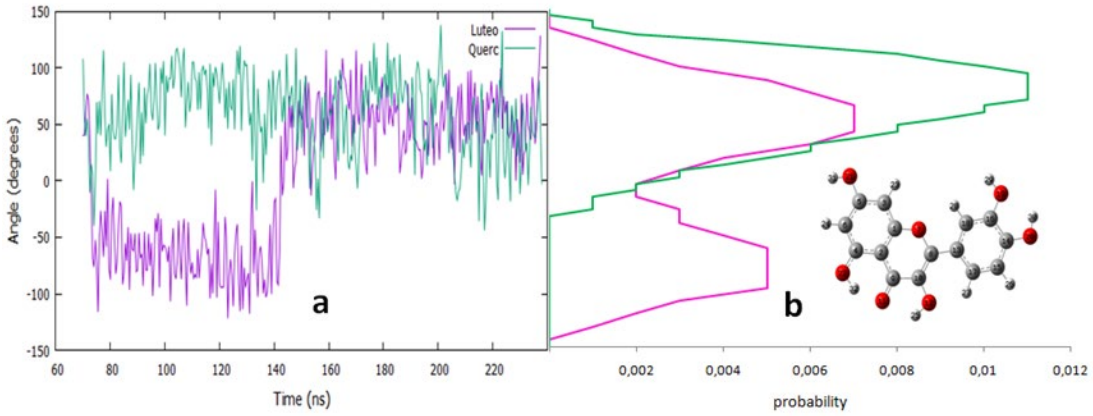

Figure 3. a: The time variation of the intramolecular dihedral angle between the pyrone double A-, C-ring with respect to the catechol B-ring of the Luteo and Querc flavonoids in the membrane environment. **b:** The corresponding dihedral-angle distribution is seen to the right with the presentation of the Querc molecular structure depicted in the inset.

The plots in Figure 3 show clearly the different conformational dynamics of the two flavonoids in the membrane environment. The extra phenolic hydroxyl -O(12)-H(25) (see indexing of the Querc in Figure S6B) in the pyrone C-ring of quercetin, inset in Figure 3, makes the difference in the behavior of the probes, since the phenyl ring B is sterically hindered to make a full rotation.

Important information about the average orientation of the Flavonoid molecules is additionally obtained by considering the normal to the greater pyrone rings of the molecules in Figure 4. The pyrone plane normal of Luteo display a broad probability distribution between 30 to 80 degrees and a sharper distribution centered about 55 to 60 degrees is valid for Querc. These angles of the pyrone normal correspond to an average tilt of 45 degrees with respect to the membrane plane. This behavior for this sizable planar part of the molecules is obvious in Figure S5 that visualizes also the reason for that. It shows that this way is enhanced the possibility that as many as possible of the pyrone hydroxyls interact with the lipid-core /headgroup interface. The smaller catechol ring is simultaneously tilt and enters as tightly as possible inside the headgroup to obtain greatest interaction of its hydroxyls with the polar parts of the headgroup. In fact, the sharper distribution of the normal to the pyrone in Querc in Figure 4 agrees to the discussed already inability of Querc to oscillate about the planar geometry, see in Figure 3. Therefore it obtains only limited conformations in contrast to Luteo that obtains a wider repertoire of conformations about the planar geometry.

The interaction of Caffest with the polar headgroup can alternatively comprise the oxygen atoms in the two opposite tips of the molecule. The cumulative Radial Distribution Function (RDF) of the water oxygen confined in the headgroup from the oxygen atom O(1) at the ester tip of Caffest and the phenolic O(4) at the aromatic tip is shown in Figure S7B. It is clearly seen that the Caffest molecule is in average oriented with the aromatic part toward the lipid core. Furthermore, the zwitterionic polar headgroup is not affecting significantly the orientation of Caffest in the membrane. The radial distributions for the phosphate $=PO_4^{-3}$ group or the amino-group $-N(Met)_3^{+}$ closest to the above two tips O(1) and O(4) of Caffest are smaller compared to the water abundance in the neighborhood of the Caffest molecule, Figure S7C.

Finally, from Figure 2, it follows that the amount of water in the neighborhood of the probes is the largest in the case of Caffest and the flavonoids. Especially for oPhen, the influence is rather limited.

Molecular Orientation vs. Photoselection

Figure 4 shows the tdm/ DIR and the DIR/ ARN (Aromatic-Ring- Normal.) angle distributions for the Caffest and the two flavonoids. The local director, further DIR, is the inner –Z-direction of the membrane and is oriented perpendicular to the membrane surface. The tdm vector of Caffest is in average parallel to the aromatic-ring-plane. The tdm of the flavonoids lies on the pyrone plane and the tdm vector on the rigid phenanthrolines is parallel to the line between the two nitrogen atoms, Figure S8. The orientation of the tdm of the Caffest and the two flavonoid probes in the molecular frame, were obtained from Table S3.

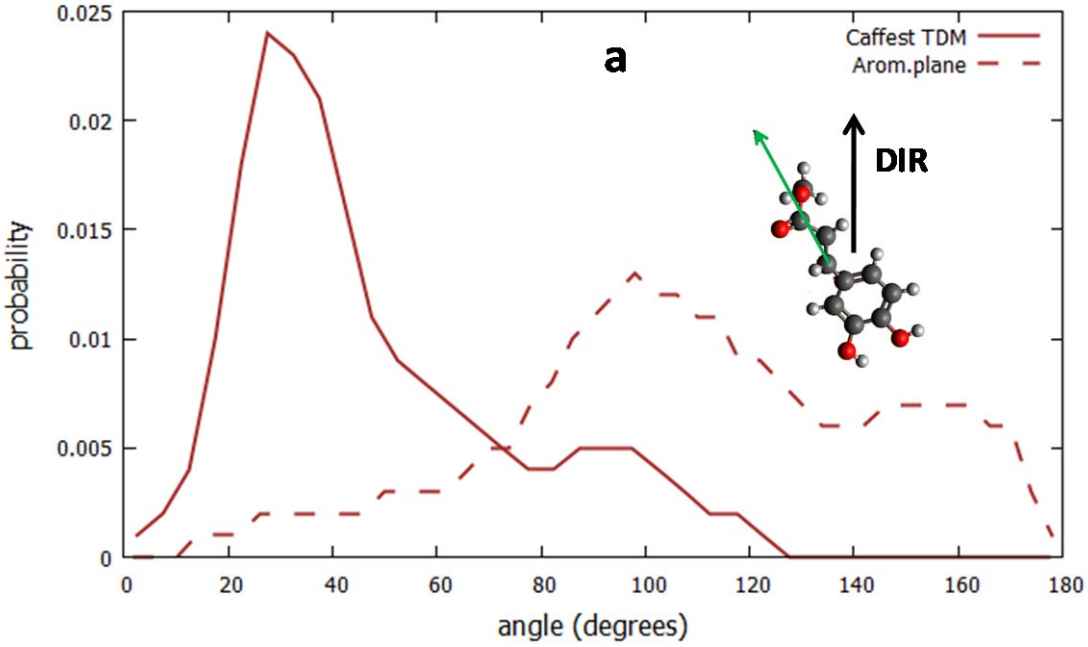
a
Caffest TDM
Arom.plane
DIR
probability
angle (degrees)
0.025
0.02
0.015
0.01
0.005
0
0
20
40
60
80
100
120
140
160
180

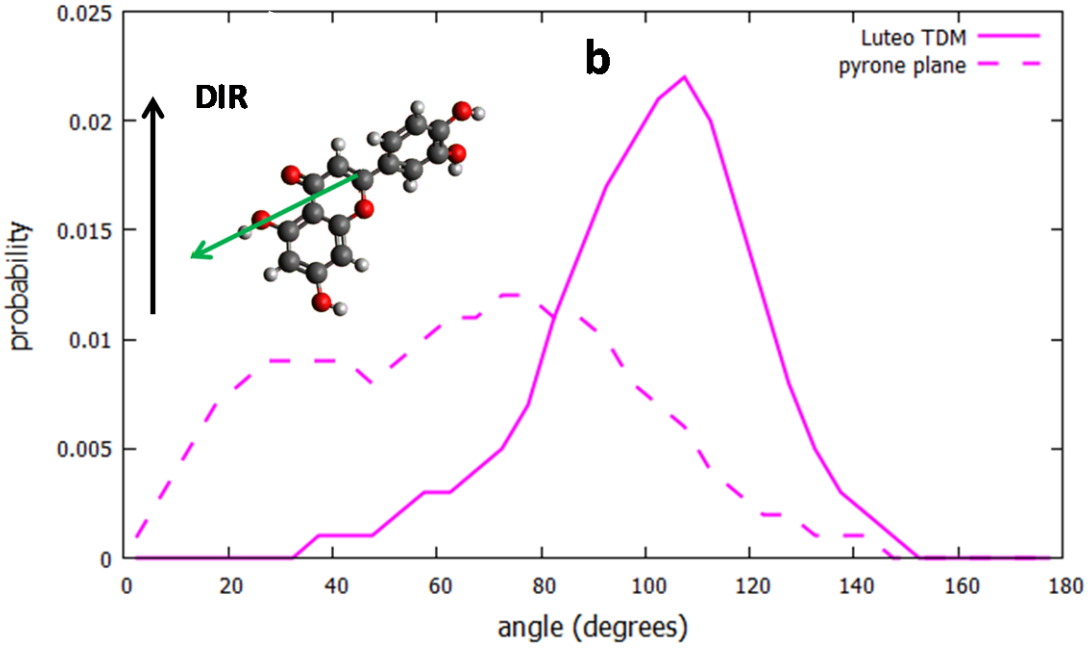
b
Luteo TDM
pyrone plane
DIR
probability
angle (degrees)
0.025
0.02
0.015
0.01
0.005
0
0
20
40
60
80
100
120
140
160
180

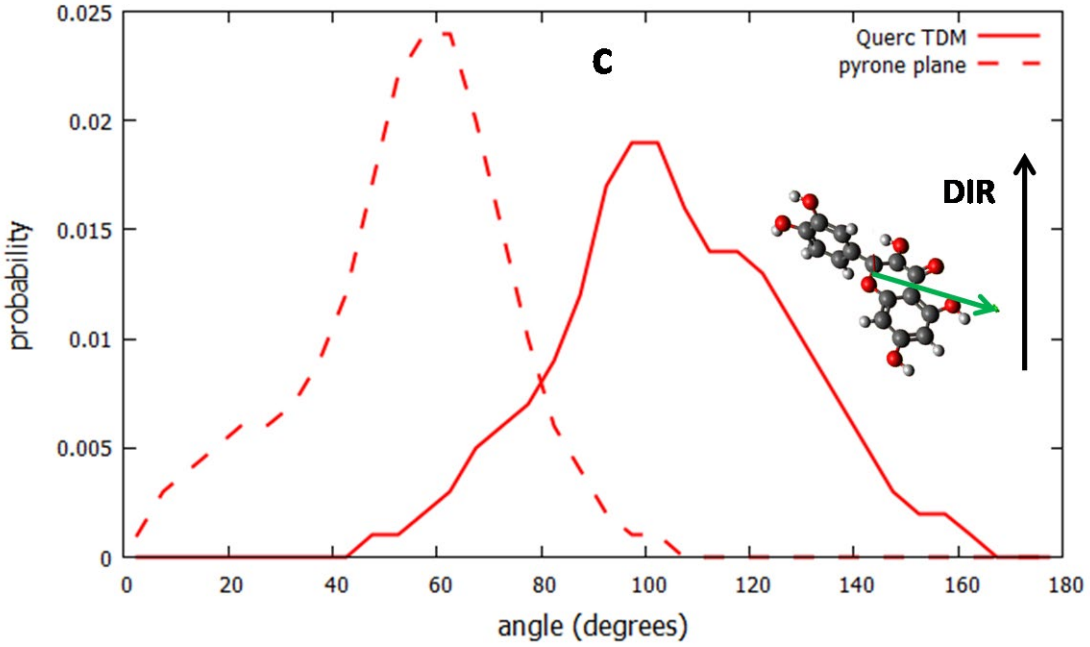

Figure 4. Combined distribution of the angle between the tdm vector (green arrow) and its normal with respect to the local director, i.e. the inner -Z-direction (further DIR) of the membrane **a.** The tdm/ DIR angle distribution for the Caffest probe (brown trace). Favonoids: **b.** The Luteo tdm/ DIR angle distribution (magenta trace) and **c.** The Querc tdm/ DIR angle distribution (red trace). Superimposed plot of the tdm/ DIR distribution for the above three drugs, Caffeast, and the two flavonoids is depicted in Figure-S9.

The excitation of a fluorescent sample of the dyes is achieved using linearly polarized light and a consequence of that is that the emission of fluorophores is anisotropic (see Ref.[58] and references therein). Therefore the most efficient photoselection in randomly oriented samples occurs for dyes that are aligned with their transition dipole moment (tdm) parallel to the polarization vector.

Comparison with experimental fluorescence photoselection intensity requires determination of the ensemble average of the cosine square of the angle between the tdm and the electric field vector[59]. The fluorescence photoselection intensity computation method is described in the supplement and presented in Table 1. The distribution $P(\vartheta)$ data of angle ϑ for each drug depicted in Figure 4 were used in the $\langle\cos^2(\vartheta)\rangle$ computation.

Fluorescent molecules with long tails are easily oriented and hindered to rotate even in rather fluid membrane environment improving the photoselection intensity by adjusting the direction of the electromagnetic irradiation[33,38]. For the smaller sized

molecules of the present work it was further assumed that the rotational correlation times of the probes is not much smaller than the fluorescence lifetime[56].

Except for Caffest, all the other probes oriented here also with their tdm approximately parallel to the membrane surface (Figure 4), with high photoselections induced by excitation beam perpendicular to the membrane surface (Table 1).

On the other hand Caffest is a smaller molecule, consisting of a single aromatic ring with two hydroxyl groups, restricting its orientation to one narrow peak, circa parallel to lipid tails. It can be seen that the Caffest molecule is in average oriented with the aromatic part toward the lipid core (Figure S7B).

The flavonoids contain two conjugated aromatic ring systems in relative motion to each other (Figure 3). They align instead perpendicular to the membrane –core/ headgroup interface with a more restricted motions than the phenanthrolines (Figure 4, Table 1). The flat geometry of these molecules is ideal for confining themselves among the acyl chains without disturbing sterically the rather significant order of the lipids close to the headgroup (Figure S4 and S5).

The normal to the aromatic rings of the Caffest probe display a wide probability preference about 80 to 120 degrees with respect to the DIR, Figure 4.

Table 1. Efficiency of the fluorescence photoselection intensity for the five antioxidant drugs of the present work calculated for angle ϑ between the transition dipole moment (tdm) and the inner membrane normal (DIR). The direction of the electric field vector of the linearly polarized incoming irradiation beam is indicated in the left column.

Electric field vector direction of the beam	**Caffest**	**Luteo**	**Querc**	**oPhen**	**Neocu**
⊥ *to membrane/* || to DIR	***probability***				
	0.52	0.14	0.19	0.21	0.23
|| *to membrane/* ⊥ to DIR	***probability***				
	0.48	0.86	0.81	0.79	0.77

Benchmarking

Before the QM/ MM calculations of the five probes in DPPC, six Time Dependent Density Functional Theory (TDDFT)[60] functionals were benchmarked against the

higher order Algebraic Diagrammatic Construction (ADC) of the polarization propagator ADC(2)-s, and ADC(3) methodologies[61].

The assessment of the appropriate density functional with two representative dyes, Caffest and Luteo, in this work was based on the data of Table S4 and settled in Table 2. The single point TDDFT computations with B3LYP[41, 42], CAM-B3LYP[50], LC-wPBE[62], ωB97XD[63] and M062X[64] functionals were performed in vacuum with the cc-pVDZ basis set. The excited state energies of oPhen in vacuum were also benchmarked by the ab-initio ADC methods as seen in Table S4.

Table 2. Electronic transition data of two of the molecules representing two of the chemical groups of this work, the methyl caffeate ester (Caffest) and luteolin (Luteo) for the flavonoids. All the shown computations were performed in vacuum with the cc-pVDZ basis set.

	caffeate methyl ester (Caffest) in			Luteolin (Luteo)		
S0 →	**Absorption from S0**					
	CAM-B3LYP	***ADC(2)***	***ADC(3)***	***CAM-B3LYP***	***ADC(2)***	***ADC(3)***
→ S1	283 (0.64) H→ L	281(0.61) H→L	276 (0.27) H→L	297 (0.40) H→ L	315 (0.00) H-5 →L	296 (0.40) H→L
→ S2	256 (0.03) H→L+1	263(0.07) H→ L+1	268 (0.47) H→ L	281 (0.00) H-4 → L	302 (0.29) H→L	274 (0.06) H-1→L
→ S3	250 (0.00) H-2→L+1	262 (0.00) H-3→L+1	237 (0.00) H-3→L	272 (0.12) H-1 → L	281 (0.18) H-1→L	-
→ S4	212 (0.43) H-1→L	-	-	261 (0.01) H-2 → L	-	-

The TDDFT CAM-B3LYP functional computation shows rather good agreement in the transition energy and the oscillatory strength with the ADC(3) result of the first excited state of Caffest. The M062X and the ωB97XD TDDFT functionals of Table 2 show also a comparable agreement to the ADC(2) as the CAM-B3LYP methods. The ADC(2) result for the first excited state of Caffest comprises a reasonably good agreement with the CAM-B3LYP computation, too. The latter was therefore selected for further spectral investigation. The current study lies in line with previously published lipid membrane studies of similar systems[35], in which this long-range corrected functional was also preferred. From Table 2, the transitions to the first excited state in the TDDFT of Caffest benchmarking are all occurring between HOMO to LUMO frontier orbitals. Also for Luteo, the first excited state has a HOMO to LUMO assignment, which is confirmed by the higher order ADC calculations.

One and Two Photon Spectroscopy

The OPA spectra of the relatively small dyes in the present work fall in the UV region of the electromagnetic spectrum. However, the reduction of the irradiation frequency to its half in the TPA spectroscopy moves the absorption to the (infra−) red region of the electromagnetic spectrum. The advantage of using TPA spectroscopy in a biological environment is two-fold: the use of two IR photons is less harmful to the cell while the three -dimensional resolution of the confocal microscopy is enhanced and the penetration depth is increased[58].

The global OPA and the TPA spectra of the probes shown in Figure 5 is the simulated superimposition of the 40 uncorrelated snapshots using two different approaches. In the first one, the selected molecular structures of the probes ~~taken~~ from the MD simulation have been subjected to the QM treatments without their lipid environment (VAC, in blue), while in the second one (EMB, in red) the lipid membrane environment was taken into account through an electrostatic QM/MM hybrid computation. The results of the two approaches were further compared and analyzed to assess the effects of the environment on the energetics, transition dipole moments and oscillator strengths or TPA strengths of the probes.

The global OPA bands in Figure 5 appear in the UV region, while the TPA spectra, regularly less energetic with wavelength from 543 to 717 nm, belong to the visible region of the electromagnetic radiation. Both OPA and TPA involve rather broad transition bands and while the OPA bands have approximately equal total width in VAC and EMB conditions, the EMB TPA are generally broader than in VAC. In both the OPA and the TPA area the EMB runs have greater intensity than the VAC spectra. In addition, the DPPC membrane seems to enhance the OPA spectra of o-Phen, and the TPA spectra of Luteo, Neocu, and Querc. From all compounds considered here, the o-Phen probe is located the closest to the membrane center, and its ground to excited state dipole moment is therefore the least influenced by the polar groups, which are located at the edges of the membrane. For the other three probes, the transition state dipole moments in between the excited states are more enhanced by the neighboring polar groups. This is emerging the most for Luteo, whose distance to the water layer is the closest.

The appearance of the OPA spectra with a width from 67 nm to 139 nm from Neocu to Caffest, is in general less complex than the TPA spectra, Figure 5. The most

complex OPA spectrum is the Caffest in VAC with a double top at 322 and 353 nm and two shoulders at 272 and 400 nm. The other molecules exhibit single OPA bands from 263 in Neocu to and 300 nm in oPhen in the VAC with small closely related EMB bands. Also the EMB band of the Caffest is single at 363 nm.

Table S5 in the Supplement depicts all the OPA and TPA transitions in detail.

Making use of the number of snapshots, we focus on the two allowed OPA transitions with the outer lying highest and lowest energy. They can be considered as representatives of the MM environment causing substantial shifts in the optical wavelengths and the optical properties in general. The discrimination of the effect of the membrane environment on the probes can be observed in the OPA and TPA transition impulses that were convoluted with Gaussian lineshapes and superimposed simulating the spectral bands in Figure 5.

OPA Spectra

The OPA transitions are first displayed and discussed. The TPA spectra based on the OPA energies are further computed, displayed and evaluated. By considering the same frame of the outliers in VAC and in EMB conditions (Table S6) the difference in the properties of both the above OPA and TPA spectra can be associated to either the electrostatic interactions with the membrane or to the outlier conformation.

As seen with fluorescent probes like DPH embedded in DPPC, water can affect the transition frequencies and might lead to a red shift[37]. This effect of the headgroup water is observed in all but one (Querc) OPA spectra of the five dyes in the present work in embedded conditions compared to the vacuum (See Table 3).

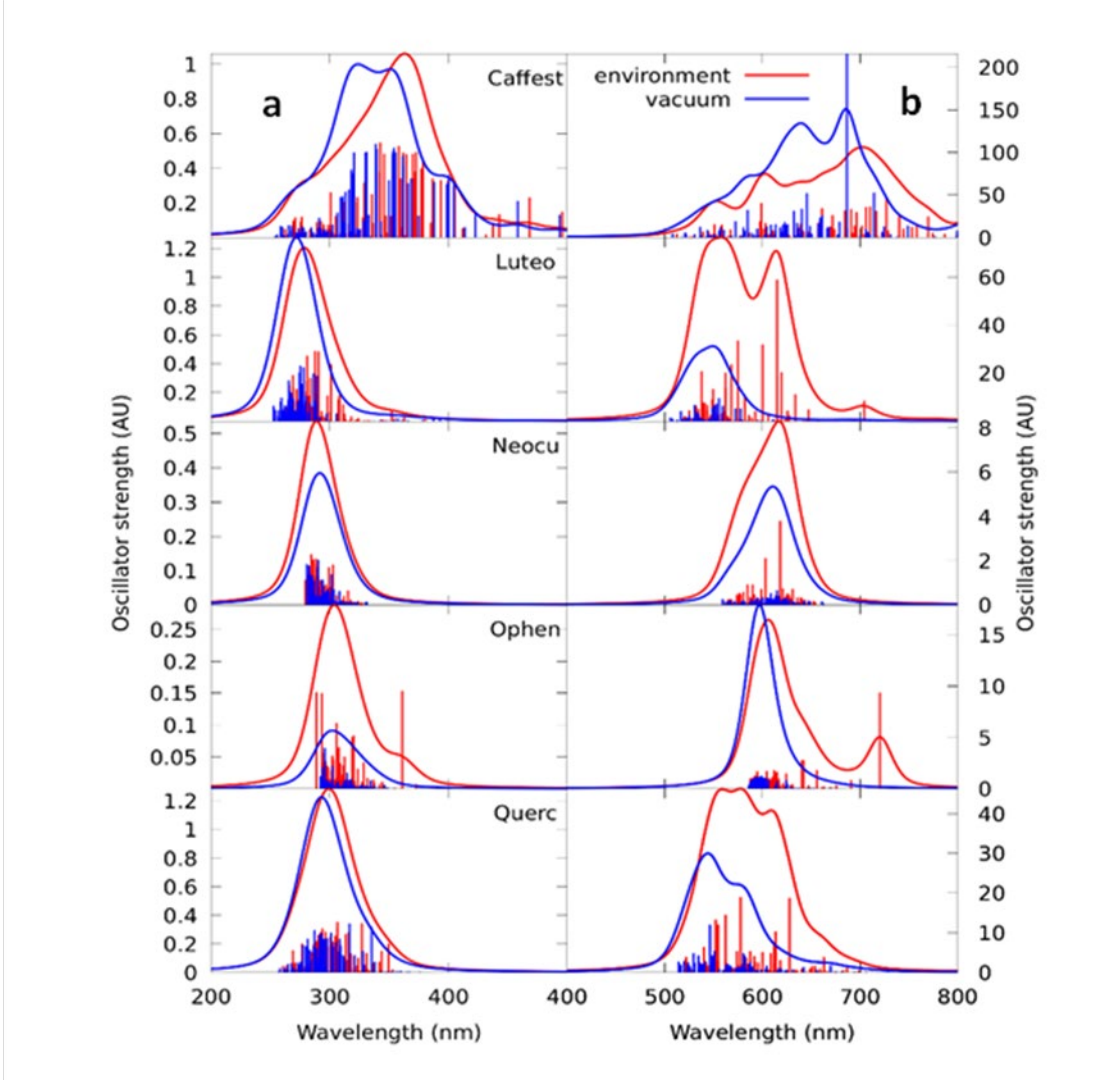

Figure 5. Superimposed OPA (a) and TPA (b) impulse global spectra and their Gaussian convolutions of the 40 MD time frames. The computations were performed either in vacuum (blue lines) or in the membrane environment (red lines), see text for details.

In **Table 3** the wavelengths and the oscillator strengths of the OPA transitions are depicted for the outliers of Caffest and the two flavonoids. The so-called Λ-overlap parameter of Peach et al.[65] is given as well. Transitions which exhibit Λ-values which are smaller than 0.4 are expected to display charge transfer character. In general, for the calculations in which the embedding is taken into account, the Λ-overlap in the table decreases, while its values stay consistently larger than the above critical value. Only for the EMB cases of both flavonoids, a slightly smaller value than 0.5 is found. Using orbital depictions in Figure 6, the possible charge-transfer character can be visualized through the involved occupied and virtual frontier orbitals. For Querc, the latter (virtual) ones seem to obtain a charge excess in the "higher right" catechol B-

ring, while the previous (occupied) ones exhibit strong contributions from the "lower left" A-, C- ring pyrone complex. Regular localized transitions for Neocu and Caffest are shown in Figure S10A and S10D respectively.

Table 3. Optical properties of the methyl caffeate ester (Caffest) and the flavonoid (Luteo, Querc) outliers identified in the OPA spectra. Wavelengths are given in nm, the magnitudes of dipole moments in Debye (Db) units and the TPA cross sections sigma of the two-photon absorption in GM units[66]. The probes are considered both embedded in the electrostatic QM/ MM DPPC model membrane environment (EMB) and in absence of the lipid environment (VAC). In parentheses is the oscillator strength of the strongest transition component and in brackets the Λ–overlap parameters of Peach et al.[65]. Also the TPA related excited state dipole moments (edm) S1,1 and the excited states transition state dipole moments (tdm) S1,2 are presented in the same table[35].

Caffest						
VAC						
FRAME	**TPA sigma/ GM**	**S0,0/Db**	**S1,1/Db**	**S1,2/Db**	**λ/nm**	**Transition S0→S1 / Db**
low FRQ	6.21	6.74	3.27	3.44	534.3 (0.12) H >L	1.51 [0.67]
high FRQ	12.3	3.51	5.89	0.546	319.4 (0.22) H >L	1.54 [0.61]
EMB						
low FRQ	11.1	8.72	4.24	2.38	572.8 (0.13) H >L	1.58 [0.61]
high FRQ	16.0	4.53	6.73	0.680	309.4 (0.21) H >L	1.52 [0.57]
FLAVONOIDS[1]						
Luteo						
VAC						
FRAME	**TPA sigma/ GM**	**S0,0**	**S1,1**	**S1,2**	**λ/nm**	**Transition[1] S0→S2/ Db**
low FRQ	7.35	1.81	1.94	0.419	276.5 (0.14) H >L, H-1> L	1.54 [0.66]

high FRQ	0.457	2.42	2.424	0.434	266.8 (0.08) H-1 >L, H-3 >L	0.91 [0.57]
EMB						
low FRQ	31.9	9.38	1.60	1.32	301.2 (0.25) H >L	1.98 [0.49]
high FRQ	0.830	8.01	2.30	0.136	267.3 (0.17) H >L+1, H> L+2, H-1 >L	1.44 [0.61]
Querc						
VAC						
FRAME	**TPA sigma/ GM**	**S0,0/ Db**	**S1,1/Db**	**S1,2/ Db**	**λ/nm**	**Transition[1] S0→S2/Db**
low FRQ	1.33	5.892	1.638	0.478	320.9 (0.10) H >L	1.13 [0.67]
high FRQ	0.0912	8.317	2.605	0.412	280.9 (0.12) H >L	1.20 [0.61]
EMB						
low FRQ	3.95	7.82	1.60	1.52	331.2 (0.13) H>L, H >L+1	1.22 [0.47]
high FRQ	0.890	9.19	2.37	0.164	269.0 (0.13) H-1>L, H-2>L+1	1.17 [0.67]

[1] The first non dark-transitions of the Flavonoids Luteo and Querc were the S0 → S2.

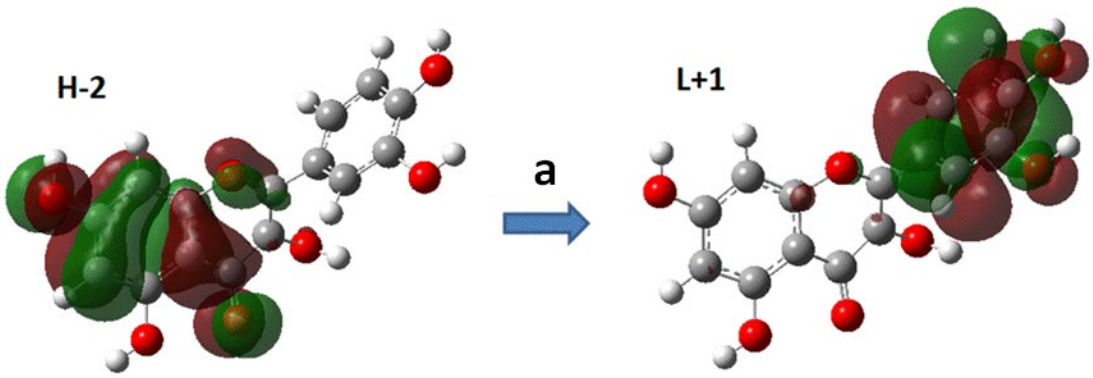

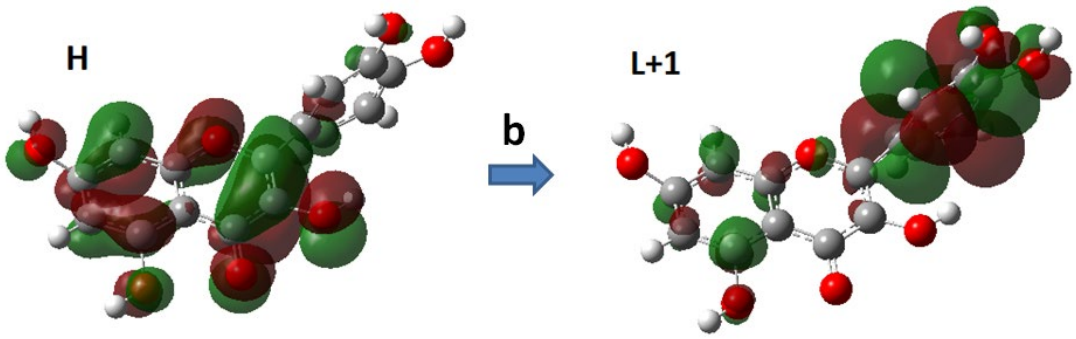

Figure 6. Demonstration of the EMB Querc S0 → S2 OPA outlier "charge-transfer" transitions based on the molecular geometry of the corresponding high and low frequency snapshots. **a:** High frequency 269 nm HOMO-2 → LUMO+1. **b:** Low frequency 331 nm HOMO → LUMO+1.

An outstanding difference from 1.8 to 9.4 Db between VAC and EMB simulations is observed in Table 3 between the ground state dipole moment in the Luteo probe for the low frequency outliers. This is an effect of the interaction of the Luteo with the headgroup water, Figure 7, where this molecule is seen to attract strongest than any of the other probes the water molecules. On the contrary, phenanthrolines display a reduced ability to approach efficiently the polar (water) zone of the membrane.

Also, the difference between the high to low frequency wavelength of the EMB Caffest outliers between 309 nm to 573 nm is unique among the other molecules. This difference is only a conformation dependent effect as also the VAC high and low frequency outliers give comparable wavelength difference values, Figure 8a.

These cases concern the most flexible of the probes, the Caffest and the flavonoids in particular. On the contrary, the rigidity of the Neocu probe is one reason why the differences between the molecular properties in VAC or EMB conditions are rather insignificant, Table S8. Furthermore, Neocu is confined mostly away from the headgroup due to higher lipid affinity. The high hydrophobicity of the Neocu probe is the reason that molecular properties in EMB is almost the same to those of VAC as it is found quite deep in the membrane, away from the headgroup region. The high frequency outlier properties of Neocu are similar for oPhen because it is also less amenable to deformation than the other three probes. The low frequency oPhen outlier, however, shows a significant difference in the properties with or without the membrane environment. This depiction of the outlier shows that the more exposed

than for Neocu, nitrogen atoms of oPhen are amenable to electrostatic interaction with the polar headgroup. Both the low and high frequency outlier of oPhen reside closer to the headgroup with the nitrogen tips oriented towards the headgroup compared to Neocu whose position and orientation are the opposite. In particular also the low frequency outlier of oPhen shows one of the nitrogen tips of the molecule well inside the headgroup and the Neocu clearly further away from the headgroup (Figure S5).

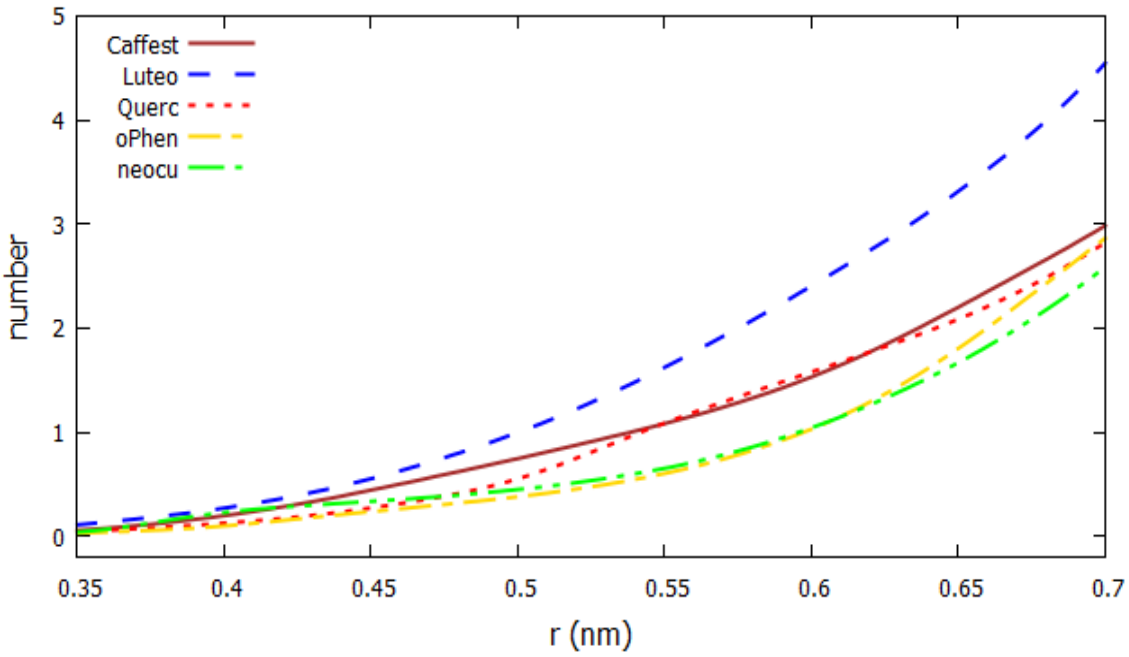

Figure 7. The short-range polar interaction of the dyes to the headgroup water of the DPPC bilayer. The Luteo molecule seems to attract the greatest number of water molecules.

The extra environmental sensitivity of the low frequency outliers compared to the high frequency ones is also true for the flavonoids and Caffest phenolic molecules. They possess several polar extremities in the form of oxo-groups and phenolic hydroxyls. In particular the low frequency outliers of these groups show red shift indicating that the reorganization of the molecular structure is also important for the reduced electronic gap of the excited states due to deformations which result from membrane-probe interaction.

As seen in the spectrum of the Caffest in Figure 8a the low frequency EMB outlier has the double red shift compared to the shift of the high frequency outlier. This difference can be attributed to the extreme twist of the esterified tail of the molecule

of the low frequency outlier seen in Figure S5, depicting the Caffest in the membrane framework. Both the esterified and the phenolic oxygen extremes of the flexible Caffest molecule are occasionally in the position to interact with the polar headgroup groups and the headgroup water. The increased length of the frontier π-orbitals of the probe leads to low transition energy while the extreme steric and electrostatic exposure of this low frequency outlier to the electrostatic environment results to greater shift of the embedded case.

Allowed S0 → S1 OPA transitions were observed for the Caffest while the flavonoids showed only strong S0 → S2 transitions instead (Table 3). The phenanthrolines displayed stronger OPA transitions only to the higher S0 → S3 or S4 excited states Figure S11. The analyses for Caffest and the Flavonoids are given here, while the ones for the phenanthrolines can be found in SI (Table S8).

The One Photon Absorption (OPA) spectra of the Caffest outliers are shown in Figure 8a and the corresponding two flavonoids' Luteo and Querc spectra are shown in Figure 8b and 8c, respectively. Red shift is observed in the OPA spectra for the Caffest and the Luteo probes when embedded in the lipid membrane compared to VAC, while the Querc probe is the only species that shows a significant blue shift of the high frequency outlier in EMB conditions. This is due to the hindrance of the rotation around the pyrone-catechol junction (see Figure S5 and S6) along with the discussions there) and the subsequent inability of the Querc species to obtain an overall planar configuration with a fully extended conjugated double-bond system throughout the molecule. As indicated in Figure S6B, an extra hydroxyl –O(12)H(25) can indeed be seen which hinders the intramolecular dihedral angle. The motional dynamics of the molecules in the membrane environment was necessary to reveal the exceptional behavior of Querc. The frontier π-orbitals involved in the OPA transitions of the idealized planar conformers of the two flavonoids shown in Figure S12**A** do not show any particular difference that could explain the unique blue shift of Querc.

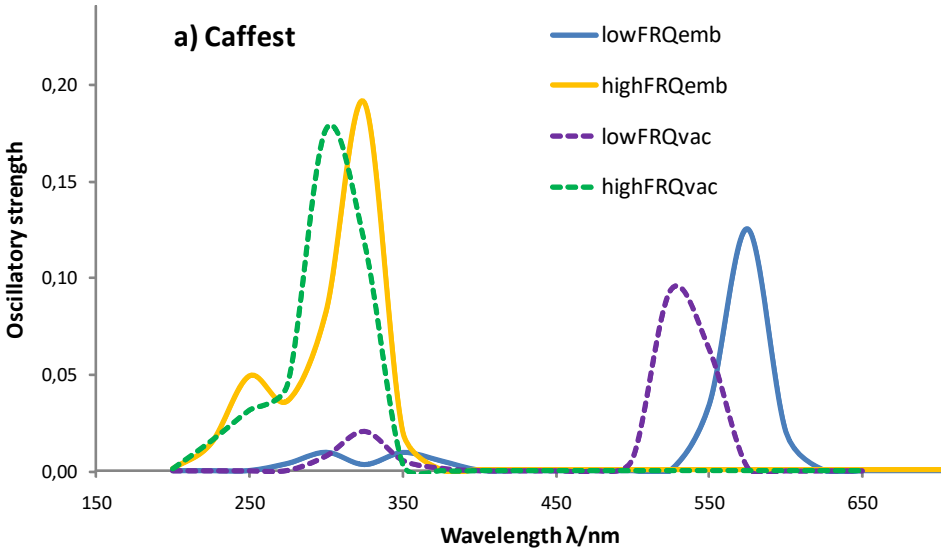
a) Caffest
lowFRQemb
highFRQemb
lowFRQvac
highFRQvac
Oscillatory strength
0,20
0,15
0,10
0,05
0,00
150
250
350
450
550
650
Wavelength λ/nm

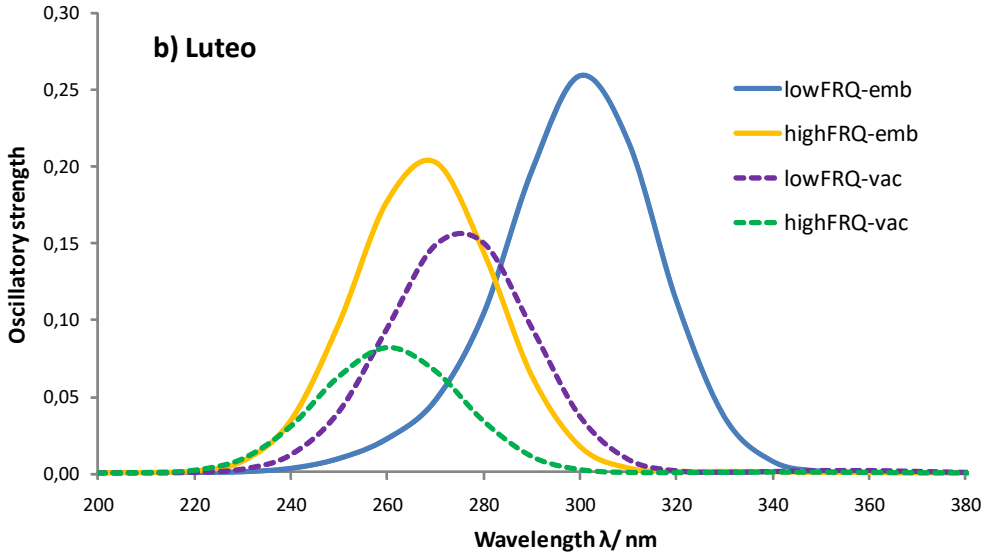
b) Luteo
lowFRQ-emb
highFRQ-emb
lowFRQ-vac
highFRQ-vac
Oscillatory strength
0,30
0,25
0,20
0,15
0,10
0,05
0,00
200
220
240
260
280
300
320
340
360
380
Wavelength λ/ nm

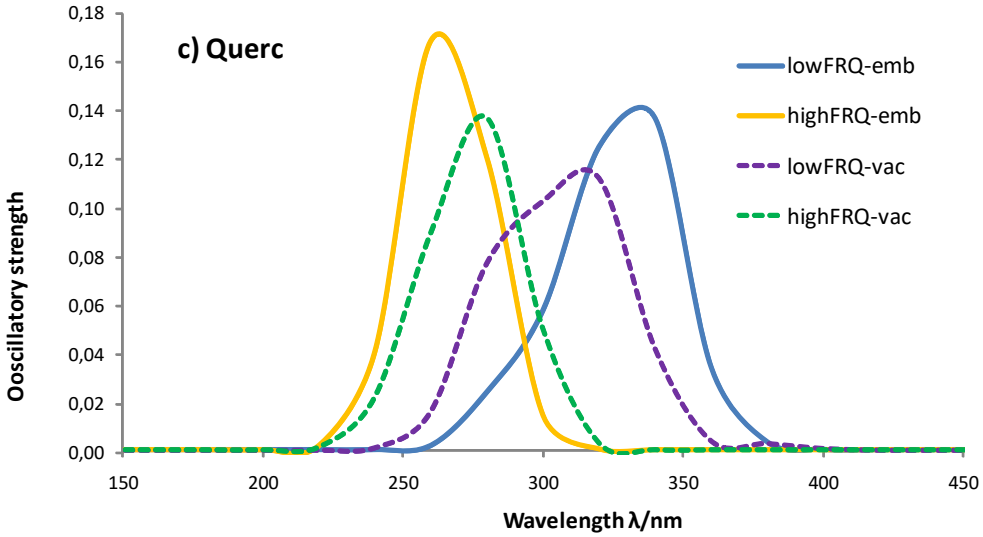

Figure 8. Gaussian convolution of the OPA transition impulses Half Width at Half Height (HWHH) 33.30 nm for (a) Caffest, (b) Luteo and (c) Querc.

a) Caffest S0→ S1 transitions. The lowest frequency frame had wavelength λ = 573 nm and the highest frequency frame had wavelength λ = 309 nm (see as well Table 3). The flavonoids S0 → S2 transitions for Luteo in **b)** with lowest transition energy frame at λ = 301 nm and a highest transition energy frame wavelength λ = 267 nm. In **c)** Querc with lowest energy transition of-frame wavelength λ = 331 nm and the frame with the highest energy transition had wavelength λ =269 nm.

The OPA outlying frame S0→S1 transition bands of Caffest involve only HOMO to LUMO orbitals as shown in Figure S10D in the supplement. However, the OPA spectra of Caffest in Figure 8a are rather complicated: the convolutions incorporate also the weaker but still allowed transitions of the outliers, which involve higher lying excited states. As a consequence of these secondary transitions, the structure of the outlier bands is altered.

Accordingly, from Figure 8, it can be seen that the EMB probe displays a 50 nm red shift in the low frequency outliers compared to the VAC. For the high frequency outliers, the red shift is still visible although it diminishes now to one half of the previous value. These values differ from the ones of Table 3, where data about individual lines are given, as Figure 8 is rather a Gaussian weighted convolution.

The transitions of the low frequency outliers display a spread of 210-250 nm. In particular the low frequency of Caffest outlier in VAC in Figure 8a, obtains a bump at

about 317 nm, in the region of the high frequency area. This is an indication that the low frequency outlier conformation has also a secondary high- frequency transition component. The conformation reliance of the bump is reinforced by the appearance of the same bump in the low frequency EMB outlier, where it is a bit broader and split. It proves the effect of the membrane environment on the molecular conformation.

As see in Figure 8a the high frequency OPA Caffest spectrum in vacuum contains at least one of the peaks of the Methyl Caffeate of Wang et al.[67] around at 213 and 300 nm. For example the band at the 300 nm present in our panoramic OPA absorption spectrum in Figure 5 is also identically present at the high frequency outlier of Figure 8a, which in addition has a shoulder at ca 250 nm.

Compared to the Caffest OPA spectra with the relatively sharp and well defined transitions (Figure 8a) the spectra of flavonoids are more diffuse with significant superimposition of the low with the high frequency outliers (see Figure 8b and 8c) for Luteo and Querc. It depends on the flexible structure of the relatively sizable flavonoid molecules, and on the nature of the allowed S2 state transition compared to the S1 in Caffest.

A significant red shift of 24 nm from the VAC to the EMB probe for the low frequency outlier of Luteo was observed compared to the much smaller 6 nm red shift of the high frequency outlier in Figure 8b. The low frequency shift is a consequence of the interaction of Luteo with the headgroup water layer enabling a conformation change which extends the conjugated double bond system (see Figure S5). As seen in the radial distribution functions given in Figure 7, Luteo is the probe that interacts the strongest with the headgroup water among all the five probes of this work. However, the most distorted conformers of the flavonoids appear to be the ones in the high frequency frames (Figure S5), where the distortion of the molecule from planarity shortens the conjugated double bond system.

Two main transitions of the UV spectrum of Luteolin at 356 and 264 nm are reported in fig. 2 of Dong et al.[68]. In our work the panoramic Luteo OPA fluorescent spectrum of our Figure 5 consists in a single band at ca 270 nm, while the vacuum OPA snapshot in Figure 8b contains a low and a high frequency top between 260 and 275 nm, which agrees with the article of Dong et al., while the 356 top of that article is absent from our spectra.

The low frequency outlier of Querc obtains also a significant red shift of 22 nm (Figure 8c). In addition a blue shifted shoulder by almost the double wavelength of 42 nm appears in the low frequency outlier in VAC. In contrast to all the other red shifted bands of Caffest and flavonoids, a unique, significant, 17 nm blue shift for the high frequency outlier of Querc can be observed from the VAC to the EMB environment.

The panoramic OPA spectra of Querc in Figure 5 display a broad absorption band at ca 300 nm. However, in our Figure 8c snapshots in vacuum two separate bands at 270 and 320 nm are displayed. As depicted in fig. 2 of the work by Zhou and Tang[69], quercetin showed two absorption bands in the UV. The first in the 300–400 nm range and the second in the 240–280 nm range representing the cinnamoyl system (B and C rings) and the benzoyl system (A and C rings), respectively. In particular Quercetin shows two bands at 280 and 330 nm in very good agreement with the low and high frequency snapshots of the OPA fluorescent absorption in our work.

From Figure 2 in Xu et al.[70] the absorption peaks of o-phenanthroline are found at 229 and 264 nm. The panoramic OPA fluorescence spectra of oPhen in our Figure 5 and in particular the VAC or EMB snapshots in Figure S11 show instead a broad band at ca 250 to 330 nm, reaching the higher wavelength edge of the experimental result.

TPA Spectra

The background data for the TPA cross section computations by eq. (3) are the excited states dipole moments (edm) and the transition states dipole moments (tdm). Considering the ground to excited state dipole moments which give rise to the OPA spectra, it was also important to determine the S1 excited state dipole moments and the transition dipole moments for the S1 $\rightarrow$ S2 transitions.

We focus here on the computed values for Caffest and the flavonoids. The edm $\langle S1|\mu|S1\rangle$ and the tdm $\langle S2|\mu|S1\rangle$ for the S1 $\rightarrow$ S2 transitions of the outliers of the OPA spectra for Caffest are shown in Figure 9. In general, the membrane environment in the realm of the headgroup affects the edm and the tdm of Caffest in the opposite way since from VAC to EMB conditions the first one increases while the second one decreases. The high frequency outlier shows the exception, displaying instead a slightly increased tdm value from VAC to EMB conditions. Compared to the

location of the probe among the lipid tails in the other snapshots, this outlier is located close to the polar water layer (see Figure S7B and S7C). The effect points at the importance of the environment. The molecule here is oriented ‘up right’, i.e. perpendicular to membrane surface, which enables an interaction of the water molecules along the orientation of the tdm.

The edm and tdm of the OPA outliers of the two flavonoids (see Figure 8) are displayed in Figure 9. As the Caffest, both flavonoids are always confined in the realm of the headgroup interacting strongly with the polar lipid-core/ headgroup interface. Their behavior is therefore similar as they are both flexible and they also contain active polar phenolic oxygen atoms. The edm of the first excited state of both molecules decreases slightly in the EMB condition compared to VAC. This is opposite to the Caffest, which is smaller, not amenable to major reorganization. The largest difference of the excited state dipole moments of the two groups however is the much greater span of the Caffest, ca. 7 Db, compared to the ca. 2.5 Db of the flavonoids. The tdm between S1 and S2 of the high frequency outliers for both the Luteo and the Querc probes is decreasing in EMB conditions as was also observed in the Caffest. On the contrary the tdm of the low frequency outliers of the flavonoids is instead increased by means of the interaction with the polar membrane headgroup, a trend opposite to Caffest.

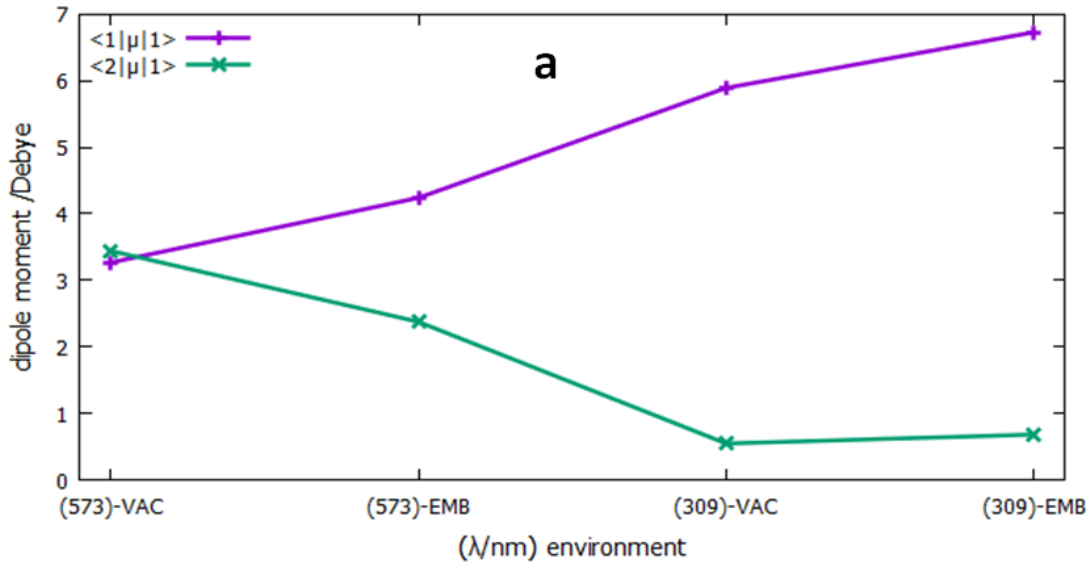

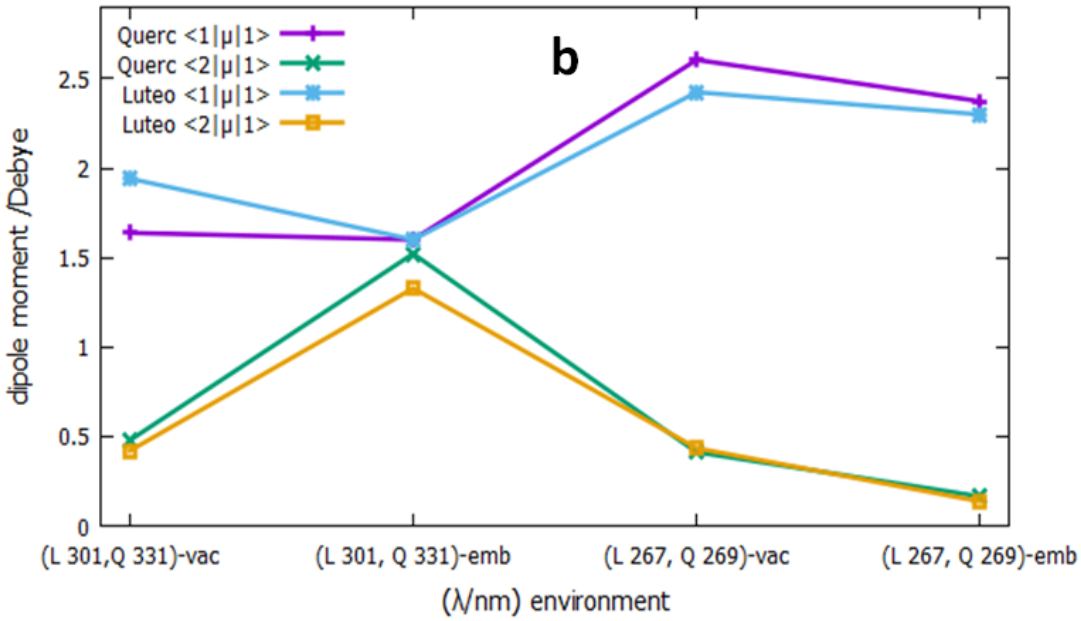

Figure 9. The magnitudes of the excited state dipole moments (edm) and transition dipole moments (tdm) of the two most outlying frames (outliers) of the Caffest and the two flavonoids in EMB environment or in VAC. The numbers in parenthesis in the abscissa label in nm the wavelengths of the outliers. The ordinate denotes the magnitudes of the matrix elements of the dipole moment in Debye's (Db). The lines are drawn to guide the eye.

a) Caffest: The Low Frequency outlier (573) and the High Frequency outlier (309) of Caffest, respectively, correspond with the molecular snapshots in Figure S2. The purple curve (+) depicts the edm ⟨S1|μ|S1⟩ of the first excited states while green curve (×) depicts the tdm ⟨S2|μ|S1⟩ between the two excited states 2 to 1.

b) Flavonoids: Low Frequency outliers (L 301, Q 331) and the high frequency outliers (L 267, Q 269) outliers, respectively, for Luteo (L) and Querc (Q). The purple (+) and the blue curves (squares) depict the edm ⟨S1|μ|S1⟩, while green (×) and the orange curves (squares) depict the tdm ⟨S2|μ|S1⟩ of the probes.

Conclusions

The position and orientation of five anti-oxidant organic molecules embedded in a DPPC membrane at room temperature are investigated using extended Molecular Dynamics calculations, including lateral diffusion constant D, area per lipid, average thickness. Their response to incident light is investigated and their use in fluorescent microscopy is evaluated. By means of hybrid quantum mechanics – molecular mechanics (QM/MM) calculations, the one- (OPA) and two-(TPA) photon absorption

spectra of these molecules are investigated and the influence of the membrane on the spectra is discussed.

The spectroscopic properties of two flavonoids, luteolin and quercetin, are very similar concerning the OPA and TPA transitions, despite a few significant differences. The at first sight small difference of the extra phenolic hydroxy- group of the pyrone ring in quercetin, which is missing in luteolin, results in the existence of two different conformations of the latter. On the contrary due to the steric hindrance of the extra hydroxyl which prevents a rotation around the pyrone/catechol junction, the quercetin probe is found to stabilize in the membrane with the above two planar sections twisted by a ca. 90 degrees dihedral angle. As a consequence, among the here presented molecules, quercetin is the only one which gives a blue shifted OPA spectrum in a membrane environment. The computational analysis of the conformation of this molecule shows that the conjugated double bond system cannot extend on the entire molecular body.

The caffeate methyl ester and the flavonoids remain close to the lipid-core/headgroup interface. In contrast to the phenanthrolines which reside closer to the membrane center, caffeate methyl ester and the flavonoids interact strongly with the water content of the polar head group. Luteolin is the most hydrophilic molecule among the five probes.

The current study demonstrates the influence of the environment on embedded anti-oxidants of particular kind like flavonoids. Throughout the calculation of the (non-) linear optical properties of the five molecules, the impact of the anisotropic environment on the ground- to excited state transition dipole moments and the state dipole moments is visualized. This influence can be attributed to inherent conformational changes of the molecules along the molecular dynamics process modulating the local environment. To analyze spectroscopic experiments in biological environments, it is therefore of utmost importance to carefully examine the position and orientation of the molecular probes.

The here presented work is a first step to investigate the embedding of transition metal complexes (work in process) and further multiscale modeling studies are needed to get insight in their time-dependent properties in biological membranes. In the longer term, the current study can therefore shed light on changing membrane properties like softness or fluidity.

The present methodology enables one to study the involvement of the cell membrane in the cell protection from strong oxidation agents like hydrogen peroxide in presence of naturally occurring traces of labile iron and/or copper ions. It can reveal the mechanism allowing for certain antioxidant drugs to penetrate cell membrane and chelate metal ions isolating them from the nucleus and preventing DNA damage and cell death. Numerous natural compounds chemically related to the five dyes studied here, are known to prevent oxidative stress related diseases. Oxidative damage can lead e.g. to formation of AD-specific pathological β-amyloid plaques to elderly people that lose part of the natural antioxidant resistance. Our method can help current pharmaceutical developments of improved antioxidants, including hybrid molecules [71, 72], very important for treatment of neurodegenerative disorders, cancer, atherosclerotic vascular diseases etc.

Supporting Information

The Supplementary Information (SI) part describes the Molecular Dynamics (MD) simulations conditions highlighting the general properties of the DPPC membrane such as: thermodynamic Phase, Area per Lipid, Order Parameter and Lateral Diffusion constant of the lipids. The probe/ headgroup interaction was visualized by choosing certain characteristic snapshots of the MD trajectories relating the molecular orientation to photoselection. The rotation barrier of the intramolecular dihedral rotation angle between the constituent planar parts of the two flavonoids was determined interpreting their observed different behavior in the MD simulations. Radial Distribution Functions (RDF's) were constructed measuring the Caffest and the Flavonoids approach range to the headgroup water molecules and to the polar parts of the headgroup. Finally, part of the computations data of the two Phenanthrolines was outlined.

Author contributions

N.P.B., M.P., S.K.: Calculations, design of the project, redaction of the article

Declaration of Competing Interest

The authors declare that they have no known competing financial interests or personal relationships that could have appeared to influence the work reported in this paper.

Acknowledgement

N.P. Benetis is grateful to the Swedish Infrastructure Committee (SNIC) and acknowledges the computational time granted in the projects SNIC 2021/6-68 and 2021-1-43, 'Large-scale bio and materials modeling across spatial and temporal scales' of P.I. Prof. Aatto Laaksonen. The Flemish Supercomputer Centre (VSC) (Flanders, Belgium) and the Herculesstichting (Flanders, Belgium) are acknowledged for the computational time on the Tier-1 cluster Breniac. M.P. acknowledges the support from the Ministry of Education, Youth and Sports of the Czech Republic (ERDF/ ESF "Nano4Future" Grant CZ.02.1.01/0.0/0.0/16_019/0000754).

N. P. Benetis expresses also his many thanks to his teachers in new quantum chemistry methods, Prof. Aatto Laaksonen and Prof. Heribert Reis.

References

(1) Zhao Z. Iron and Oxidizing Species in Oxidative Stress and Alzheimer's Disease. *Aging Medicine*. **2019**, *2*, 82–87

(2) Cameron, R.B.; Beeson, C.C. ; Schnellmann, R.G. Development of Therapeutics that Induce Mitochondrial Biogenesis for the Treatment of Acute and Chronic Degenerative Diseases. *J. Med. Chem.* **2016**, *59*:*23*, 10411–10434

(3) Lage, S.L.; Pinheiro, A.E.; Hilligan, Kerry L.; Laidlaw, E.; Rupert, A.; Namasivayan, S.; Rocco, J.; Galindo, F.; Kellogg, A.; Kumar, P.; et al. Persistent Oxidative Stress and Inflammasome Activation in $CD14^{high}CD16^{-}$ Monocytes From COVID-19 Patients. *Front. Immunol.* **2022**, *12,* 799558

(4) Panche, A. N.;, Diwan, A. D. ; Chandra1, S. R. Flavonoids: an Overview. *J. of Nutrit. Sci.* **2016,** *5:47*, 1 -15

(5) Zhang, W.; Zeng, Z.; Wei,J. Electrochemical Study of DPPH Radical Scavenging for Evaluating the Antioxidant Capacity of Carbon Nanodots *J. Phys. Chem.* C **2017**, *121*, 18635−18642

(6) Halliwell B.; Gutteridge M.C. Free Radicals in Biology and Medicine. *Oxford University Press* 3rd Edt. 1999

(7) Saija, A.; Scalese, M.; Lanza, M.; Marzullo, D.; Bonina, F.; Castelli, F. Flavonoids as Antioxidant agents: Importance of their Interaction with Biomembranes. *Free Radic. Biol. and Medic.* **1995,** *19*:4, 481-486.

(8) Antropova, I.G.; Revina, A.A. ; Kurakina, E.S.; Magomedbekov E.P. Radiation Chemical Investigation of Antioxidant Activity of Biologically Important Compounds from Plant Materials. *ACS Omega* **2020**, *5*, 5976−5983

(9) Scheidt, H. A.; Pampel, A.; Nissler, L.; Gebhardt, R.; Huster, D. Investigation of the Membrane Localization and Distribution of Flavonoids by High-Resolution Magic Angle Spinning NMR Spectroscopy. *Biochim. et Biophys. Acta* **2004**, *1663,* 97– 107.

(10) Melidou. M.; Riganakos, K. ; Galaris D. Protection Against Nuclear DNA Damage Offered by Flavonoids in Cells Exposed to Hydrogen Peroxide: The Role of Iron Chelation. *Free Radic. Biol. & Medic.* **2005**, *39***,** 1591 – 1600.

(11) Nousis, L.; Doulias, P.T.; Aligiannis, N.; Bazios, D.; Agalias, A.; Galaris, D.; Mitakou, S. DNA Protecting and Genotoxic Effects of Olive Oil Related Components in Cells Exposed to Hydrogen Peroxide. *Free Radic. Res.* **2005**, *39*, 787–795.

(12) Leopoldini, M.; Russo, N.; Chiodo, S.; Toscano, M. Iron Chelation by the Powerful Antioxidant Flavonoid Quercetin. *J. Agric. Food Chem.* **2006,** *54*, 6343-635.

(13) Netto, L.E.; Antunes, F. The Roles of Peroxiredoxin and Thioredoxin in Hydrogen Peroxide Sensing and in Signal Transduction, *Mol. Cells* **2016**, *39,* 65–71.

(14) Rodriguez-Morato, J.; Xicota, L.; Fito, M.; Farre, M.; Dierssen, M.; de la Torre, R. Potential Role of Olive Oil Phenolic Compounds in the Prevention of Neurodegenerative Diseases, *Molecules* **2015**, *20*, 4655–4680.

(15) Barbouti, A.; Doulias, P.-T. ;. Zhu, B.-Z ; Frei, B.; Galaris, D. Intracellular Iron, but not Copper, Plays a Critical Role in Hydrogen Peroxide-Induced DNA Damage. *Free Rad. Biol. Med.* **2001**, *31*, 490−498.

(16) Doulias, P.-T.; Christoforidis, S.; Brunk, U.; Galaris, G. Endosomal and Lysosomal Effects of Desferrioxamine: Protection of HeLa Cells From Hydrogen Peroxide-Induced DNA Damage and Induction of Cell Cycle Arrest. *Free Radic. Biol. Med.* **2003,** *35*, 719–728.

(17) Alimi, L.O.; Alyami, M.Z.; Chand, S.; Baslyman W.; Khashab, N.M. Coordination-Based Self-Assembled Capsules (SACs) for Protein, CRISPR–Cas9, DNA and RNA Delivery. *Chem. Sci.* **2021**, *12*, 2329- 2344

(18) Ma, Z.; Jacobsen, F.E; Giedroc, D.P. Coordination Chemistry of Bacterial Metal Transport and Sensing. *Chem. Rev.* **2009**, *109*, 4644–4681

(19) Truong, D.H.; Nhung, N.T. A.; Dao, D.Q. Iron Ions Chelation-Based Antioxidant Potential vs. Pro-oxidant Risk of Ferulic Acid: A DFT Study in Aqueous Phase. *Comput. and Theor. Chem.* **2020**, *1185*, 112905

(20) Shao, B.; Mao, L.; Tang, M.; Yan, Z-Y.; Shao, J.; Huang, C-H.; Sheng Z-G. Zhu, B-Z. Caffeic Acid Phenyl Ester (CAPE) Protects against Iron-Mediated Cellular DNA Damage through Its Strong Iron-Binding Ability and High Lipophilicity. *Antioxid.* 2021, *10:798*, 1-20

(21) Cable, H.; Lloyd, J.B. Cellular Uptake and Release of Two Contrasting Two Iron Chelators. *J. Pharm. Pharmacol.* **1999**, *51*, 131–134.

(22) Boumans, H.; van Gaalen, M.C.; Grivell, L.A.;. Berden, J. A Differential Inhibition of the Yeast Bc1 Complex by Phenanthrolines and Ferroin. Implications for Structure and Catalytic Mechanism. *J. Biol. Chem.* **1997,** *272,* 16753–16760.

(23) Kitsati, N.; Mantzaris, M.D.; Galaris, D. Hydroxytyrosol Inhibits Hydrogen Peroxide-Induced Apoptotic Signaling via Labile Iron Chelation. *Redox Biol.* **2016**, *10*, 233-242.

(24) Plotnikov, M.B.; Plotnikova, T. M. Tyrosol as a Neuroprotector: Strong Effects of a "Weak" Antioxidant. *Curr Neuropharmacol.* **2021,** *19:4*, 434–448.

(25) Kitsati, N.; Fokas, D.; Ouzouni, M.D.; Mantzaris, M.D.; Barbouti, A.; Galaris, D. Lipophilic Caffeic Acid Derivatives Protect Cells Against H_2O_2-Induced DNA Damage by Chelating Intracellular Labile Iron. *J. Agric. Food Chem.* **2012**, *60,* 7873–7879.

(26) Mantzaris, M.D.; Bellou, S.; Skiada, V.;Kitsati, N.; Fotsis, T.; Galaris, D. Intracellular Labile Iron Determines H_2O_2-Induced Apoptotic Signaling via Sustained Activation of ASK1/JNK-p38 Axis. *Free Radic. Biol. Med.* **2016**, *97*, 454–465

(27) Ren, J.; Meng, S.; Lekka, Ch.E.; Kaxiras, E. Complexation of Flavonoids with Iron: Structure and Optical Signatures, *J. Phys. Chem. B* **2008**, *112*, 1845-1850.

(28) Oliver, M.; Adrover, M. ; Frontera, A.; Ortega-Castro, J.; Miró, M. In-Vitro Prediction of the Membranotropic Action of Emerging Organic Contaminants Using a Liposome-Based Multidisciplinary Approach. *Science of the Total Environ*. **2020,** *738,* 140096.

(29) Ploeg, P. van der; Berendsen, H.J.C.; Molecular Dynamics Simulation of a Bilayer Membrane. *J. Chem. Phys*. **1982**, *76*, 3271-3276.

(30) Hennel J. W.; Klinowski J.. Magic Angle Spinning: A Historical Perspective. Klinowski J. (ed.) New Techniques in Solid-State NMR. *Top. Cur. Chem. 246*, 1–14 Springer, Heidelberg 2005.

(31) Arora, A.; Byrem, T.M.; Nair, M.G.; Strasburg. G.M. Modulation of Liposomal Membrane Fluidity by Flavonoids and Isoflavonoids. *Archiv of Biochem. and Biophys.* **2000**, *373:1*, 102-109.

(32) van Meer, G.; Voelker, D. R.; Feigenson, G. W. Membrane Lipids: Where they are and How they Behave. *Nat. Rev. Mol. Cell Biol*. **2008**, *9*, 112−124.

(33) Paloncýová, M.; Aniander, G.; Larsson, E.; Knippenberg, S. Cyanine Dyes with Tail Length Asymmetry Enhance Photoselection: A Multiscale Study on DiD Probes in a Liquid Disordered Membrane. *Spectrochim. Acta Part A Mol. Biomol. Spectrosc.* **2020**, *224*, 117329.

(34) Knippenberg, S.; Osella, S. Push/Pull Effect as Driving Force for Different Optical Responses of Azobenzene in a Biological Environment. *J. Phys. Chem. C* **2020**, *124*, 8310–8322.

(35) Osella, S.; Murugan, N. A.; Jena, N. K.; Knippenberg, S. Investigation into Biological Environments through (Non)linear Optics: A Multiscale Study of Laurdan Derivatives. *J. Chem. Theory Comput.* **2016**, *12*, 6169−6181.

(36) Osella, S.; Di Meo, F.; Murugan, N.A.; Fabre, G.; Ameloot, M.; Trouillas, P.; Knippenberg, S. Combining (Non)linear Optical and Fluorescence Analysis of DiD To Enhance Lipid Phase Recognition. *J. Chem. Theory Comput.* **2018**, *14*, 5350–5359.

(37) Osella, S.; Paloncýová, M.; Sahi, M.; Knippenberg, S. Influence of Membrane Phase on the Optical Properties of DPH. *Molecules* **2020,** *25*, 4264

(38) Osella, S.; Knippenberg, S. Triggering On/Off States of Photoswitchable Probes in Biological Environments. *J. Am. Chem. Soc.* **2017**, *139*, 4418−4428.

(39) Abraham, M.J.; Murtola, T.; Schulz, R.; P´all, S.; Smith, J.C.; Hess, B.; Lindahl, E. GROMACS: High Performance Molecular Simulations through Multi-Level Parallelism from Laptops to Supercomputers, SoftwareX **2015**, *1–2*, 19–25.

(40) Frisch, M. J.; Trucks, G. W.; Schlegel, H. B.; Scuseria, G. E.; Robb, M. A.; Cheeseman, J. R.; Scalmani, G.; Barone, V.; Petersson, G. A.; Nakatsuji, H.; et al Gaussian, Inc., Wallingford CT, 2016.*Gaussian 16 Rev. C.01*, *Wallingford, CT*, 2016.

(41) Becke, A. D. Density-Functional Thermochemistry. III. The Role of Exact Exchange. *J. Chem. Phys.* **1993**, *98*, 5648−5652.

(42) Lee, C.; Yang, W.; Parr, R. G. Development of the Colle- Salvetti Correlation-Energy Formula into a Functional of the Electron Density. *Phys. Rev. B: Condens. Matter Mater. Phys*. **1988**, *37*, 785−789.

(43) Dunning, T. H. Gaussian Basis Sets for Use in Correlated Molecular Calculations. I. The Atoms Boron through Neon and Hydrogen. *J. Chem. Phys.* **1989**, *90*, 1007−1023.

(44) Chiu, S.-W.; Pandit, S.A.; Scott, H.L;. Jakobsson, E. An Improved United Atom Force Field for Simulation of Mixed Lipid Bilayers. *J. Phys. Chem. B* **2009**, *113*, 2748-2763.

(45) Hess, B.; Bekker, H.; Berendsen, H. J. C.; Fraaije, J. G. E. M. LINCS: A Linear Constraint Solver for Molecular Simulations. *J. Comput. Chem.* **1997**, *18*, 1463−1472.

(46) Darden, T.; York, D.; Pedersen, L. Particle mesh Ewald: An N·log(N) Method for Ewald Sums in Large Systems. *J. Chem. Phys.* **1993**, *98*, 10089−10092.

(47) Nosé, S. A Unified Formulation of the Constant Temperature Molecular Dynamics Methods. *J. Chem. Phys.* **1984**, *81*, 511−519.

(48) Hoover, W. G. Canonical Dynamics: Equilibrium Phase-Space Distributions. *Phys. Rev. A* **1985**, *31*, 1695−1697.

(49) Aidas, K.; Angeli, C.; Bak, K.L.; Bakken, V.; Bast, R.; Boman, L.; Christiansen, O.; Cimiraglia, R.; Coriani, S.; Dahle, P.; et al. The Dalton Quantum Chemistry Program System. *Wiley Interdiscip. Rev. Comput. Mol. Sci*. **2014**, *4*, 269-284.

(50) Yanai, T.; Tew, D. P.; Handy, N. C. A New Hybrid Exchange−Correlation Functional using the Coulomb-Attenuating Method (CAM-B3LYP). *Chem. Phys. Lett.* **2004**, *393*, 51−57.

(51) Cronstrand, P.; Luo, Yi; Ågren H. Multi-Photon Absorption of Molecules. *Advanc. Quant. Chem.* **2005***, 50*, 1.

(52) Albota, M.; Beljonne, D.; Brédas, J.L.; Ehrlich, J.E.; Fu, J.Y.; Heikal, A.A.; Hess, S.E.; Kogej, T. ; Levin, M.D.; Marder, S.R.; et al. Design of Organic Molecules with Large Two-Photon Absorption Cross Sections. *Science* **1998***, 281*, 1653−1656.

(53) Dreuw, A.; Polkehn, M.A.; Binder, R.; Heckel, A.; Knippenberg, S. Computational Design of Improved Two-Photon Active Caging Compounds Based on Nitrodibenzofuran. *J. Comput. Chem.* **2012,** *33*, 1797−1805.

(54) Paloncýová, M.; Berka, K.; Otyepka, M. Convergence of Free Energy Profile of Coumarin in Lipid Bilayer. *J. Chem. Theory Comput.* **2012**, *8*, 1200−1211.

(55) Paloncýová, M.; Fabre, G.; DeVane, R. H.; Trouillas, P.; Berka, K.; Otyepka, M. Benchmarking of Force Fields for Molecule- Membrane Interactions. J. Chem. Theory *Comput.* **2014**, *10*, 4143− 4151.

(56) Knippenberg, S.; Fabre, G.; Osella, S.; Di Meo, F.; Paloncyova, M.; Ameloot, M.; Trouillas, P. Atomistic Picture of Fluorescent Probes with Hydrocarbon Tails in Lipid Bilayer Membranes: An Investigation of Selective Affinities and Fluorescent Anisotropies in Different Environmental Phases. *Langmuir* **2018**, *34*, 9072–9084.

(57) Filipe, H.A.L.; Sousa, C.; Marquês J.T.; Vila-Viçosa, D.; de Granada-Flor, A. ; Viana, A.S. ; Soledade, M.; Santos, C.S.; Machuqueiro, M.; de Almeida, R.F.M. Differential Targeting of Membrane Lipid Domains by Caffeic Acid and its Ester Derivatives. *Free Radic. Biol. Med.* **2018**, *1:115,* 232-245.

(58) Walla P. J. *Modern Biophysical Chemistry Detection and Analysis of Biomolecules*, 2nd ed., Wiley-VCH Verlag GmbH & Co. KGaA, Weinheim, Germany 2014

(59) Lakowicz, J. R. *Principles of Fluorescence Spectroscopy*, 3rd ed.; Springer New York, NY 2011.

(60) Marques, M.A.L.; Ullrich, C.A.; Nogueira, F.; Rubio, A.; Burke, K.; Gross, E.K.U. eds. *Time-Dependent Density Functional Theory.* Springer-Verlag. Heidelberg 2006.

(61) Dreuw, A.; Wormit, M. The Algebraic Diagrammatic Construction Scheme for the Polarization Propagator for the Calculation of Excited States. *WIREs Comput. Mol. Sci.* **2015,** 5, 82−95.

(62) Li, H.; Nieman, R.; Aquino, A. J. A.; Lischka, H.; Tretiak, S. Comparison of LC-TDDFT and ADC(2) Methods in Computations of Bright and Charge Transfer States in Stacked Oligothiophenes. *J. Chem. Theory. Comput.* **2014,** *10 :8,* 3280–3289

(63) Chai, J.-D.; Head-Gordon, M. Systematic Optimization of Long- Range Corrected Hybrid Density Functionals. *J. Chem. Phys.* **2008**, *128*, 084106.

(64) Zhao Y.; Truhlar D.G. The M06 Suite of Density Functionals for Main Group Thermochemistry, Thermochemical Kinetics, Noncovalent Interactions, Excited States, and Transition Elements: Two New Functionals and Systematic Testing of Four M06-Class Functionals and 12 other Functionals. *Theor Chem Acc.* **2006**, *120,* 215–241.

(65) Peach, M.J.G.; Benfield, P.; Helgaker, T.; Tozer, D.J. Excitation Energies in Density Functional Theory: An Evaluation and a Diagnostic Test. *J. Chem. Phys.* **2008**, *128*, 044118.

(66) Sundholm, D.; Rizzo, A.; Jorgensen, P. Multiconfiguration Self-Consistent-Field Quadratic Response Calculations of the Two-Photon Transition Probability Rate Constants for Argon. *J. Chem. Phys*. **1994**, *101*, 4931−4935

(67) Wang W.; He P.; Liang Y.; Chen Y.; Xia A.; Zeng Q. Interaction of Anticancer Drug Methyl Caffeate with DNA Investigated by Electrochemical and Spectroscopic Methods. *ECS Trans*. **2010,** *28:18*, 79-89

(68) Dong H.; Yang X.; He J.; Cai S.; Xiao K.; Zhu L. Enhanced Antioxidant Activity, Antibacterial Activity and Hypoglycemic Effect of Luteolin by Complexation with Manganese(II) and its Inhibition Kinetics on Xanthine Oxidase. *RSC Adv*. **2017,** *7*, 53385 - 53395

(69) Zhou Y.; Tang R.-Ch. Facile and Eco-Friendly Fabrication of Colored and Bioactive Silk Materials Using Silver Nanoparticles Synthesized by Two Flavonoids. *Polymers* **2018**, *10*, 404.

(70) Xu C.-J.; Xie F.; Guo X.-Z.; Yang H. Synthesis and cofluorescence of Eu(Y) complexes with salicylic acid and o-phenanthroline. *Spectrochim. Acta A* **2005**, *61*, 2005–2008,

(71) Decker, M. Hybrid Molecules Incorporating Natural Products: Applications in Cancer Therapy, Neurodegenerative Disorders and Beyond. *Curr. Medic.l Chem*., **2011,** *18,* 1464-1475

(72) Decker M.; Krausb B.; Heilmann J. Design, synthesis and pharmacological evaluation of hybrid molecules out of quinazolinimines and lipoic acid lead to highly potent and selective butyrylcholinesterase inhibitors with antioxidant properties. *Bioorg & Medic.Chem*. **2008,** *16,* 4252–4261